Novel inhibitors of AChE and Aβ aggregation with neuroprotective properties as lead compounds for the treatment of Alzheimer's disease

Yulin Liu[a,b,1], Giuseppe Uras[c,e,1], Itse Onuwaje[d], Wenlong Li[a], Hong Yao[a], Shengtao Xu[a], Xinuo Li[a], Xinnan Li[a], James Phillips[d], Stephanie Allen[c], Qi Gong[f], Haiyan Zhang[f], Zheying Zhu[c, *], Jie Liu[b, **] and Jinyi Xu[a, ***]

[a] State Key Laboratory of Natural Medicines and Department of Medicinal Chemistry, China Pharmaceutical University, Nanjing, PR China

[b] Department of Organic Chemistry, China Pharmaceutical University, Nanjing, PR China

[c] Division of Molecular Therapeutics and Formulation, School of Pharmacy, The University of Nottingham, University Park, NG7 2RD, United Kingdom

[d] Department of Pharmacology, School of Pharmacy, University College London, London, United Kingdom

[e] Department of Clinical and Movement Neurosciences, Queen Square Institute of Neurology, University College London, London, United Kingdom

[f] CAS Key Laboratory of Receptor Research, Shanghai Institute of Materia Medica, Chinese Academy of Sciences, Shanghai, PR China

[*] Corresponding authors: Tel.: +86-25-86185283; fax: +86-25-83302827; E-mail address: jinyixu@china.com (J. Xu), cpu-jill@163.com (J. Liu), zheying.zhu@nottingham.ac.uk (Z. Zhu)

[1] Equal contribution

Abstract

A series of sulfone analogs of donepezil were designed and synthesized as novel acetylcholinesterase (AChE) inhibitors with the potent inhibiting Aβ aggregation and providing neuroprotective effects as potential modalities for Alzheimer's disease (AD). Most of the target compounds displayed effective inhibition of AChE, especially compound **24r** which displayed powerful inhibitory activity (IC_{50} = 2.4 nM). Kinetic and docking studies indicated that compound **24r** was a mixed-type inhibitor. Furthermore, in glyceraldehyde (GA)-exposed SH-SY5Y

differentiated neuronal cells, compound **24r** could potently inhibit AChE, reduce tau phosphorylation at S396 residue, provide neuroprotection by rescuing neuronal morphology and increasing cell viability. It was also found to reduce amyloid aggregation in the presence of AChE. In addition, compound **24r** showed evident protections from mitochondrial membrane dysfunction and oxidative stress in okadaic acid-induced pharmacological models. Moreover, compound **24r** exhibited more effective treatment prospects *in vivo* than donepezil, including a moderate blood-brain barrier permeability, a more potent AChE inhibitory activity and behavioral improvement in scopolamine-induced cognition-impaired mice model at a much lower dose. Collectively, compound **24r** is a promising lead compound for further investigation to discovery and development of new anti-AD agents.

Keyword

Alzheimer's disease, donepezil, sulfone group, AChE inhibitor, inhibiting Aβ aggregation, neuroprotection

1. Introduction

Alzheimer's disease (AD) is the most common progressive neurodegenerative disease [1]. Clinically, patients with AD are characterized by a full spectrum of dementia manifestations from cognitive and behavioral impairment and other neurodegenerative symptoms [2]. According to the World Alzheimer Report 2019, almost 80% of the general public are apprehensive of getting AD at some point, and a quarter think this disease not to be preventable [3]. The pathogenesis of AD is complex and still not fully understood, but several hypotheses on the pathophysiology of AD have been proposed to facilitate drug development, including low levels of acetylcholine (ACh), amyloid-β (Aβ) deposits, tau protein aggregation, oxidative stress and dyshomeostasis of biometals [4].

The cholinergic hypothesis was first proposed to explain the pathogenesis of AD and is relatively well accepted [5]. This hypothesis indicates that the pathogenesis of AD, as well as the corresponding dysfunction, are related to decreased levels of ACh [6]. As acetylcholinesterase (AChE) is the main cholinesterase (ChE) that performs 80% of hydrolytic activity in the brain, therefore, increasing levels of ACh in the brain, achieved by inhibiting AChE, is considered a good

strategy to treat AD [7]. Although there is the evidence that in advanced AD, the ratio of ACh hydrolysis is shifted toward hydrolysis mediated through butyrylcholinesterase (BuChE) when substrate inhibition of AChE takes place, which implies that inhibition of BuChE might be a promising strategy for the treatment of advanced AD, the development of AChE inhibitors is still the most successful anti-AD strategy until now [8,9]. Clinically, the current therapeutic options for AD patients are mainly limited to four AChE inhibitors (Fig. 1) including tacrine (withdraw), donepezil, rivastigmine, galantamine, huperzine A (approved by NMPA, China) and an *N*-methyl-*D*-aspartate (NMDA) receptor antagonist memantine [10]. Regrettably, while these drugs can improve symptoms of cognitive deterioration and memory loss, they cannot fully meet the needs of more patients. Therefore, there is a pressing clinical need to develop novel and more effective AChE inhibitors with additional functionality for the treatment of AD.

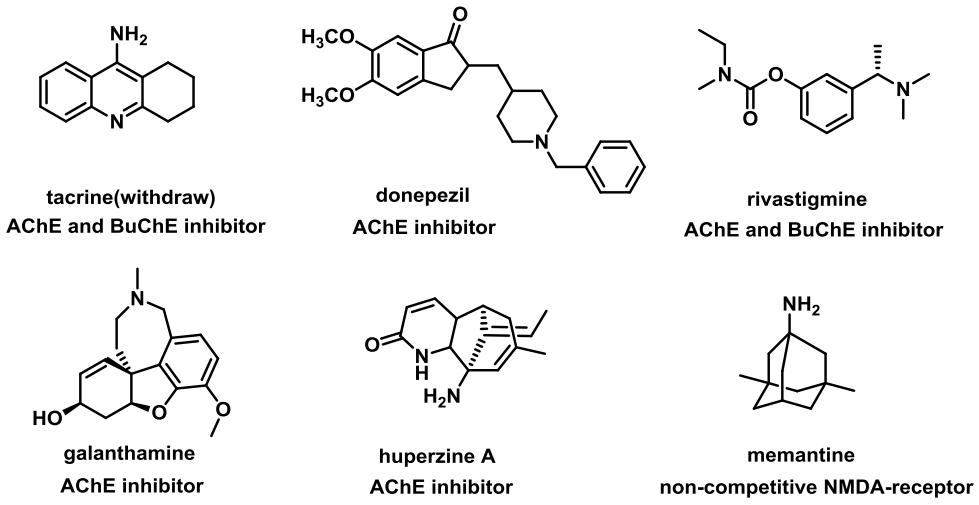

Fig. 1. Drugs approved by FDA or NMPA used for the treatment of AD.

Donepezil, as the world's best-selling anti-AD drug, belongs to the class of benzylpiperidine compounds, and is a selective AChE inhibitor administrated orally [11]. Since donepezil was successfully approved by Food and Drug Administration (FDA), much of structural modification was carried out based on it. Researchers have used the benzylpiperidine or indanone moiety as pharmacophores to fuse with other active fragments in the design of multifunctional ligands respectively [11-15]. On one hand, the most classic modification of the benzylpiperidine moiety is the introduction of *N*-benzylpyridinium moiety (Fig. 2). In 2010, Alireza Foroumadi's group

designed and synthesized a new AChE inhibitor containing *N*-benzylpyridinium fragments (compound **A**) for the first time [16]. Subsequently, a large number of *N*-benzylpyridinium AChE inhibitors were reported [17-20]. Our group also reported a class of *N*-benzylpyridinium compounds containing the skeleton of the natural product XJP [(±)-7,8-dihydroxy-3-methyl-isochroman-4-one], in which the optimal compound **B** has an AChE inhibitory activity of 0.15 nM and exhibits a good reduction of A*β* and anti-AD effects in the *in vivo* transgenic *Drosophila* model [21-23]. Regrettably, the low permeability of these *N*-benzylpyridinium compounds to the blood-brain barrier (BBB) limited their further development. On the other hand, replacing the indanone moiety of donepezil with some other heterocycles, such as diarylthiazole, purine, coumarin and ebselen to design donepezil-based multi-target directed ligands (MTDLs), led to another successful modification strategy [24-27]. Moreover, substituent modification on the benzylpiperidine moiety was another structural optimization method, especially, the incorporation of fluorine atoms. About 20% of FDA approved drugs contain at least one fluorine atom across many different drug classes [28]. The judicious introduction of fluorine can productively improve physicochemical properties, pharmacokinetic characteristics and pharmacodynamics profiles of compounds [29-31]. A systematic fluorine scan on ligands has become a routine approach in hit-to-lead optimization strategies. In 2014, Liu's research group introduced a key fluorine atom at the *para*-position of piperidine in donepezil and obtained an optimal candidate drug DC511020, which is currently in clinical phase II trials (CTR20212054). The activity of DC511020 was three times more potent than donepezil, meanwhile, it had a larger safety margin to alleviate the undesirable side effects [32].

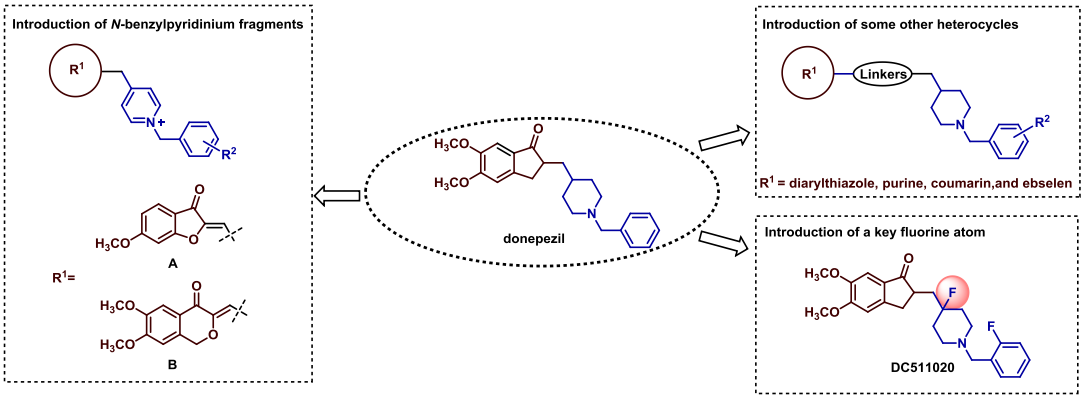

Fig. 2. Representative structures of reported donepezil-based AChE inhibitors.

Alkenyl sulfone, which is similar to chalcone, can activate Nrf2 and induce the expression of the Nrf2-dependent antioxidant enzymes, such as NAD(P)H quinone oxidoreductase 1 (NQO1) and heme oxygenase 1 (HO-1) to exert antioxidant and anti-inflammatory activity [33]. It was therefore considered as a promising neuroprotective moiety and has been applied for the design of many new neuroprotective compounds (such as **C**, **D**, **E**, **F**) for the treatment of neurodegenerative diseases (Fig. 3) [33-36]. Our aim is involved the fusion of the structure of donepezil with alkenyl sulfone in one molecule, for the first time, to synthesize a series of novel anti-AChE compounds with additional functionalities derived from antioxidant and neuroprotection, for the treatment of AD.

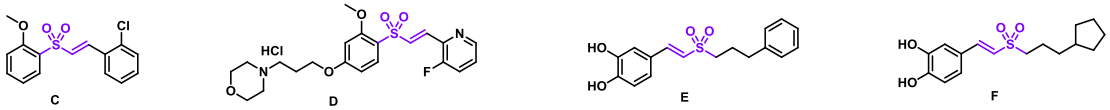

Fig. 3. Representative structures of reported neuroprotective agents containing alkenyl sulfone.

2. Result and discussion

2.1. Design and synthesis

On the basis that the antioxidant and neuroprotective effects of alkenyl sulfone are closely related to improve the pathology of AD, in this work we first introduced the alkenyl sulfone moiety, as well as sulfone moiety, into the structure of donepezil to design a class of novel donepezil analogues against AChE, aiming to alleviate the cholinergic deficit effectively for AD patients. Specifically, an alkenyl sulfone or sulfone group was introduced to replace the carbonyl of donepezil, and additionally, the ring was expanded or opened to explore the possible impact. In subsequent optimization, the introduction of fluorine atoms is expected to improve the pharmacodynamic activity and physicochemical characteristics of target compounds (Fig. 4). In our case, retention of the basic skeleton of donepezil was expected to retain a strong AChE inhibitory activity, and the replacement of carbonyl was expected to lead to antioxidant and neuroprotective activities. In order to initially verify our design strategy, a docking experiment was conducted (Fig. 6C). This structural modification allowed retention of the conformation of the compounds in the binding pocket of AChE that was basically consistent with donepezil, therefore it encouraged us to synthesize the first series of compounds.

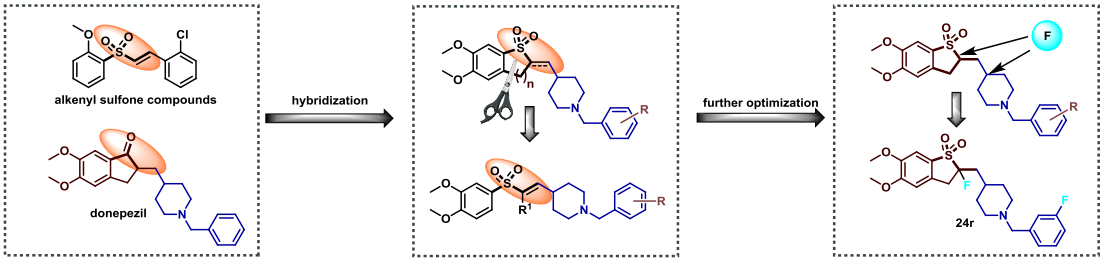

Fig. 4. Design of a series of novel compounds containing alkenyl sulfone or sulfone skeleton.

Synthesis of compounds **6a-d** is depicted in Scheme 1. Briefly, a sulfonation reaction of 1,2-dimethoxybenzene (**1a**) followed by a reduction reaction to yield compounds **3a**, which was reacted with diethyl *p*-toluenesulfonyloxymethylphosphonate to give phosphate ester intermediate (**4a**). Chlorination reaction of compound **4a** with NCS led to compound **4b** and the resulting intermediate then refluxed in methanol to give compound **4c**. Compounds **4a-c** were oxidized with *m*-CPBA to give sulfones (**5a-c**), which were reacted with 1-benzylpiperidine-4-carbaldehyde by a Wittig-Hornor reaction to produce the target products **6a-c**. Compound **6d** was synthesized by a similar strategy: compound **3a** was reacted with ethyl bromoacetate, followed by an oxidative reaction with *m*-CPBA and a Knoevenagel reaction to produce compounds **6d**.

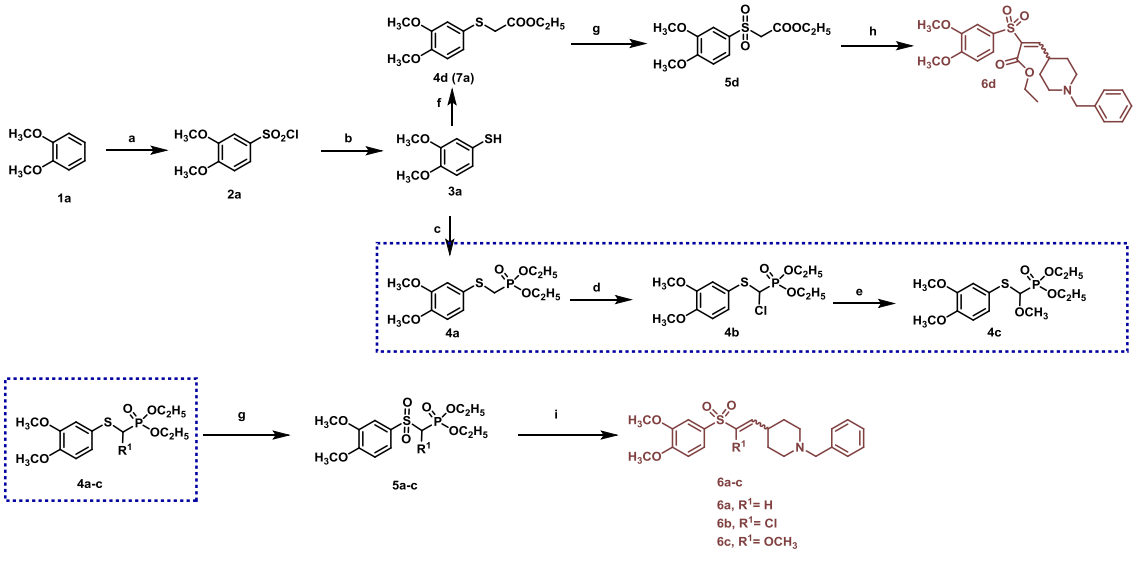

Scheme 1. Synthesis of compounds **6a-d**, reagents and conditions: (a) $ClSO_3H$, $SOCl_2$, DCM, 0 °C - rt, 91%; (b) Zn, Conc. HCl, Et_2O, EA, 85%; (c) diethyl *p*-toluenesulfonyloxymethylphosphonate, K_2CO_3, CH_3CN, rt, 63%; (d) NCS, CCl_4, rt, 72%; (e) CH_3OH, reflux, 90%; (f) ethyl bromoacetate, K_2CO_3, CH_3CN, rt, 92%; (g) *m*-CPBA (2.2

eq), DCM, rt, 78% - 91%; (h) 1-benzylpiperidine-4-carbaldehyde, piperidine (cat.), AcOH (cat.), toluene, reflux, 35%; (i) NaH, 1-benzylpiperidine-4-carbaldehyde, THF, N_2, 0 °C, 44% - 87%.

Synthesis of compounds **12a-d** is depicted in Scheme 2. Firstly, intermediates **7a-c** were hydrolyzed to produce the corresponding acids **8a-c**. Then intermediates **11a-c** were synthesized through a Friedel-Crafts acylation, a reduction reaction by Et_3Si in TFA, and an oxidation reaction by *m*-CPBA from compounds **8a-c**. Compounds **11a-c** were condensed with 1-benzylpiperidine-4-carbaldehyde to give target products **12a-c**. The *cis*-isomer and *trans*-isomer (**12a**(***Z***) and **12a**(***E***), 1:1) of **12a** could be separated by column chromatography. Finally, compound **12d** was synthesized by catalytic hydrogenation from compound **12a** to explore the activity difference between the alkenyl sulfone and sulfone substituents.

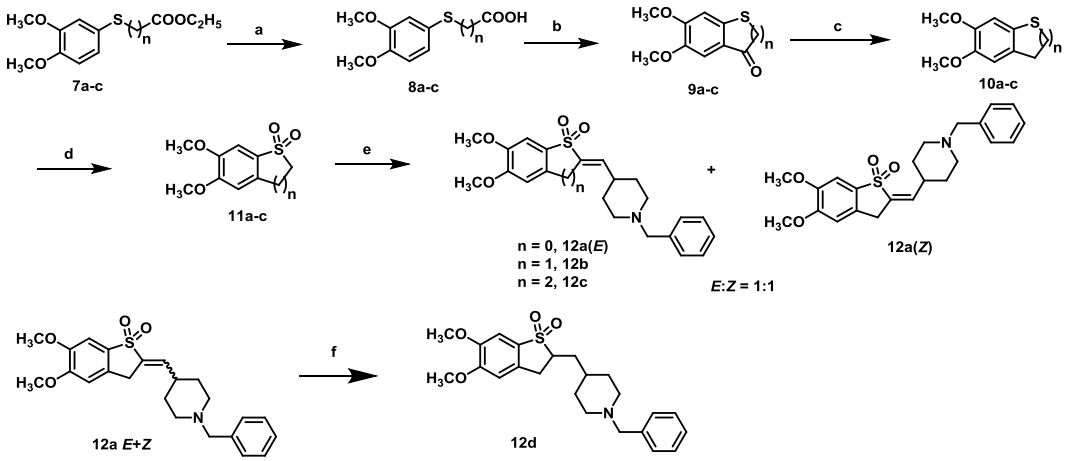

Scheme 2. Synthesis of compounds **12a-d**, reagents and conditions: (a) i) 10% NaOH aqueous, CH_3OH, 80 °C; ii) 1N HCl aqueous, rt, 88% -92%; (b) i) oxalyl chloride, DMF, 0 °C - rt; ii) $AlCl_3$, DCM, 64% - 73%; (c) Et_3Si, TFA, rt, 58% - 66%; (d) *m*-CPBA (2.2 eq), DCM, rt, 75% - 89%; (e) i) *n*-BuLi, $(CH_3)_3SiCl$, THF, -78 °C - 0 °C; ii) 1-benzylpiperidine-4-carbaldehyde, *n*-BuLi, THF, N_2, -78 °C, 22% - 26%; (f) Pd-C, H_2, CH_3OH, rt, 91%.

Synthesis of compounds **22a**, **23a** and **24a-q** is depicted in Scheme 3. The key intermediate *N*-Boc-4-fluoropiperidine-4-carbaldehyde (**16b**) shown in Scheme 3 was successfully synthesized according to Liu's work [37]. It was synthesized through a Corey-Chaykovsky reaction, a ring-opening reaction and a Swern oxidation reaction from *N*-Boc-piperidine-4-one (**13b**). Intermediate **9a** was condensed with compound **16a** or **16b** to obtain compounds **17a-b**, followed by a reduction reaction and an elimination reaction to produce intermediates **19a-b**. Compounds **19a-b** were further

oxidized to give compounds **20a-b**, which were then reduced to produce compounds **21a-b**. Finally, the target compounds **22a**, **23a**, **24a-q** were synthesized through deprotection of the Boc group of intermediates **19a**, **20a** and **21a-b** and a further reaction with diversified benzyl bromides.

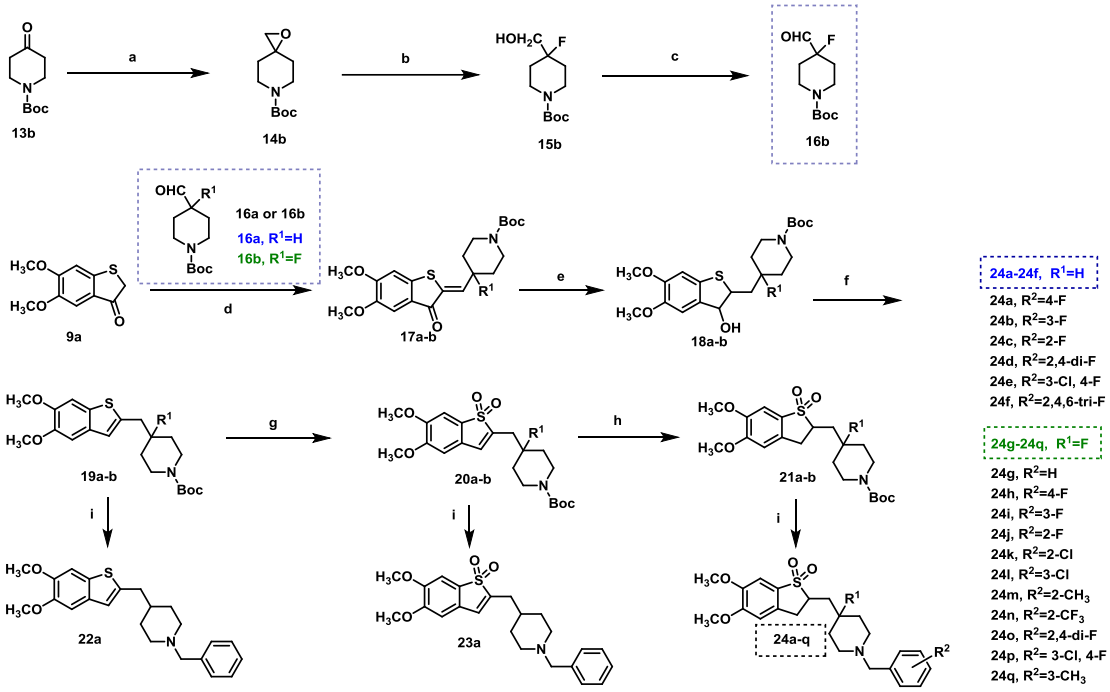

Scheme 3. Synthesis of compounds **22a, 23a** and **24a-d**, reagents and conditions: (a) *t*-BuOK, $(CH_3)_3S$=OI, DMSO, rt, 52%; (b) 70% HF-Py, DCM, rt, 77%; (c) oxalyl chloride, DMSO, Et_3N, -78 °C, 36%; (d) CH_3ONa, THF, 0 °C - rt, 62% - 68%; (e) $NaBH_4$, CH_3OH, rt, 91% - 96%; (f) NH_4Cl, CH_3OH, reflux, 86% - 91%; (g) *m*-CPBA (2.2 eq), DCM, rt, 72% - 80%; (h) Pd-C, H_2, CH_3OH, rt, 89% - 95%; (i) i) CF_3COOH, DCM, 70% - 75%; ii) different benzyl bromides, K_2CO_3, CH_3CN, rt, 45% - 66%.

Synthesis of compound **24r** is depicted in Scheme 4. Intermediate **17a** was reduced by catalytic hydrogenation to obtain compound **25a**, and then oxidized by *m*-CPBA to obtain compound **26a**, which was then reacted with NFSI reagent to obtain compound **27a**. After deprotection of the Boc group of **27a**, it was reacted with 3-fluorobenzyl bromide to afford intermediate **28a**. Subsequently, the intermediate **28a** could be successfully converted to the target product **24r** through a Barton-McCombie reaction.

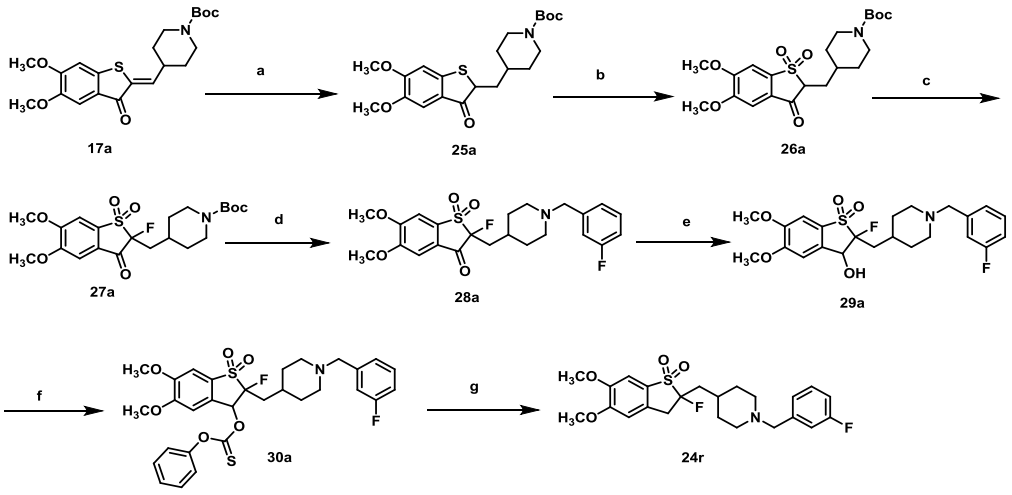

Scheme 4. Synthesis of compound **24r**, reagents and conditions: (a) Pd-C, H_2, CH_3OH, rt, 86%; (b) *m*-CPBA (2.2 eq), DCM, rt, 78%; (c) NFSI, K_2CO_3, rt, 56%; (d) i) CF_3COOH, DCM, 76% ii) 3-flurinebenzyl bromide, K_2CO_3, CH_3CN, rt, 42%; (e) $NaBH_4$, CH_3OH, rt, 84%; (f) PhOC=SCl, Py, DCM, rt, 53%; (g) BuSnH, AIBN, Tol, 120 °C, 64%.

2.2. In vitro cholinesterase inhibitory activity and SAR studies

In order to verify the effect of the introduction of the alkenyl sulfone or sulfone group on AChE inhibitory potency, we synthesized the first series of compounds **6a-e**, **12a**(***E***), **12a**(***Z***) and **12b-d**. The spectrophotometric method of Ellman was used to evaluate AChE inhibitory potency of all target compounds with donepezil hydrochloride used as a reference compound for comparison [32]. The IC_{50} values of all the first series of compounds are shown in Table 1. The results indicated that the groups on the α-position of the sulfone group have a great influence on the activities. The unsubstituted compound **6a** gave a general inhibitory activity against AChE (IC_{50} = 67.6 nM), however, the introduction of other groups such as chlorine (**6b**, IC_{50} = 340 nM), methoxy (**6c**, IC_{50} = 8437 nM) and ester (**6d**, IC_{50} ＞ 40 μM) was found to be unfavorable for the inhibitory potency. When the ring A is a five-membered ring (n = 1), the activity improves significantly, meanwhile, *trans*-isomer (**12a**(***E***), IC_{50} = 4.7 nM) is better than *cis*-isomer (**12a**(***Z***), IC_{50} = 11.1 nM). When the double bond is reduced (**12d**, IC_{50} = 4.4 nM), the inhibitory potency is equivalent to **12a**(***E***) and donepezil. When ring A is a six- or seven-membered ring (n = 2 or n = 3), the potency reduces severely (**12b** and **12c**).

Table 1. The structures and AChE inhibitory activities of the first series of compounds.

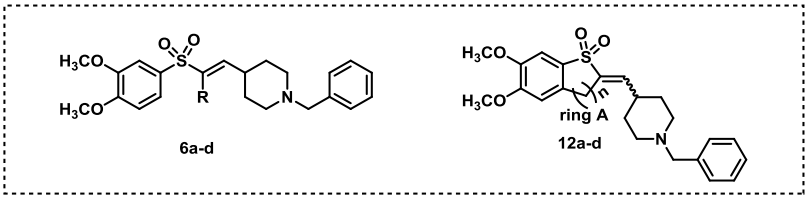

Compd.	R	n	double bound	AChE[a] IC_{50} (nM)[b] or % inhibition
6a	H	-	√	67.6 ± 2.4
6b	Cl	-	√	340 ± 26
6c	OCH_3	-	√	8437 ± 52
6d	COOEt	-	√	12.45%[c]
12a(*E*)	-	1	√	4.7 ± 0.3
12a(*Z*)	-	1	√	11.1 ± 1.2
12b	-	2	√	1820 ± 10
12c	-	3	√	32.76%[c]
12d	-	**1**	reduction	**4.4 ± 0.4**
donepezil	-	-	-	5.4 ± 0.3

[a] The zymogen of AChE was from the cerebral cortex of mouse.

[b] IC_{50}: 50% inhibitory concentration (mean ± SEM of three experiments).

[c] The data are the inhibition ratio against AChE at 40 μM.

Inspired by the potency of compounds **12d** and **12a**(***E***), we intended to further introduce substituents on the phenyl ring of benzylpiperidine for structural optimization. At the same time, taking into account that sulfone derivative **12d** could be synthesized more easily through another synthesis route, we decided to further optimize using the structure of compound **12d** as a basis. In the second series of compounds, different substituent groups were introduced to determine whether the AChE inhibitory potency could be improved. As shown in Table 2, most target compounds displayed potent inhibition towards AChE (i.e., **24a**, **24b**, **24c**, **24d**, **24e**). The *para*-fluorine

substituted derivative (**24a**, IC_{50} = 11.3 nM) and *ortho*-fluorine substituted derivative (**24c**, IC_{50} = 11.5 nM) were found to keep a moderate inhibitory potency. Out of all of the second series of compounds, *meta*-fluorine substituted derivative (**24b**, IC_{50} = 4.4 nM) was the most potent compound against AChE. In addition, double-substituted compounds (**24d**, IC_{50} = 14.7 nM and **24e**, IC_{50} = 11.5 nM) kept a moderate inhibitory potency. As a comparison, three-substituted compound (**24f**, IC_{50} = 128 nM) led to a significant decrease in inhibitory activities indicating that the number of substituents on the phenyl ring should be suitable. Derivative **22a** (IC_{50} ＞ 40 μM) and **23a** (IC_{50} = 317 nM) were compounds that fused synthesis intermediates **19a** and **20a** with a benzylpiperidine moiety respectively. Both compounds had poor inhibitory potency, indicating that two oxygen atoms of sulfone and the single bond in the ring A are critical for anti-AChE activity.

Table 2. The structures and AChE inhibitory activities of the second series of compounds.

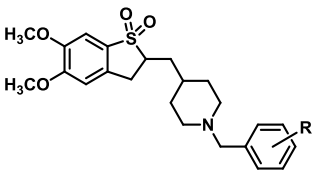

Compd.	R	AChE[a] IC_{50} (nM)[b]
22a	-	46.63%[c]
23a	-	317 ± 31
24a	4-F	11.3 ± 0.7
24b	**3-F**	**4.4 ± 0.3**
24c	2-F	11.5 ± 0.2
24d	2,4-di-F	14.7 ± 0.1
24e	3-Cl, 4-F	11.5 ± 0.9
24f	2,4,6-tri-F	128 ± 5

[a] The zymogen of AChE was from the cerebral cortex of mouse.

[b] IC_{50}: 50% inhibitory concentration (mean ± SEM of three experiments).

[c] The data are the inhibition ratio against AChE at 40 μM.

Considering that the sulfone group might lead compounds to be more polar, possibly affect its blood-brain barrier (BBB) permeability, introduction of fluorine atoms might remedy this potential problem. Therefore, we introduced fluorine atoms at the *para*-position of piperidine or the *α*-position of sulfone group in our compounds. The results are shown in Table 3. With the introduction of fluorine atoms, compounds still kept potent inhibition. Almost all compounds, whatever fluorine, chlorine or methyl on the *ortho*-, *meta*-, *para*-position (**24g**-**24m** and **24o**-**24r**) on the phenyl ring, showed strong inhibitory potency against AChE except the *ortho*-trifluoromethyl derivative **24n** (IC_{50} = 3007 nM), which lost the inhibitory activity, possibly due to the strong electron-withdrawing ability of trifluoromethyl causing the disappearance of the corresponding π-π stacking interaction. Out of all of the third series of compounds, compound **24r** (IC_{50} = 2.4 nM) with a fluorine atom at the *α*-position of sulfone group and a fluorine atom at the *meta*-position of the phenyl ring demonstrated the most potent inhibitory potency against AChE.

Table 3. The structures and AChE inhibitory activities of the third series of compounds.

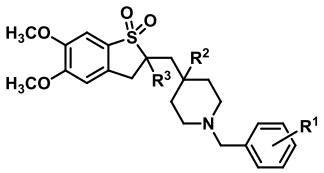

Compd.	R^1	R^2	R^3	AChE[a] IC_{50} (nM)[b]
24g	H	F	H	4.1 ± 0.1
24h	4-F	F	H	11.3 ± 0.7
24i	3-F	F	H	5.1 ± 0.3
24j	2-F	F	H	8.5 ± 0.4
24k	2-Cl	F	H	5.5 ± 0.2
24l	3-Cl	F	H	5.0 ± 0.1
24m	2-CH_3	F	H	12.1 ± 2.2
24n	2-CF_3	F	H	3007 ± 543

24o	2,4-di-F	F	H	7.1 ± 0.2
24p	3-Cl, 4-F	F	H	12.9 ± 2.1
24q	3-CH_3	F	H	3.8 ± 0.1
24r	**3-F**	**H**	**F**	**2.4 ± 0.6**

[a] The zymogen of AChE was from the cerebral cortex of mouse.

[b] IC_{50}: 50% inhibitory concentration (mean ± SEM of three experiments).

The studies so far, therefore, allowed us to obtain complete structure-activity relationships (SAR) for all compounds (Fig. 5). In summary: 1) the best activity is obtained if ring A is a five-membered ring, specifically, a five-membered ring > straight chain substituents > a six-membered ring > a seven-membered ring. 2) The sulfone group is very important for the inhibitory activity and the activity is almost completely lost when the sulfone group is removed. 3) The introduction of a double bond into ring A greatly reduces the activity and reduction of the double bond outside of ring A has a slight beneficial effect on activity. 4) The most optimal compound **24r** is obtained by introducing a fluorine atom at *α*-position of sulfone group.

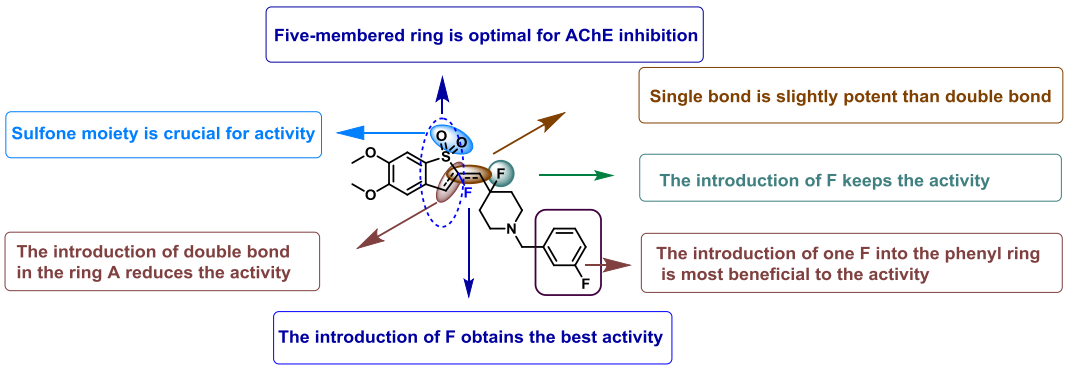

Fig. 5. The structure-activity relationships of all compounds.

2.3. Computational docking studies

To further investigate the interaction mode of compound **24r** and other representative compounds (**12a**(***E***), **12a**(***Z***) and **24b**) with recombinant human AChE (PDB code: 4EY7), we performed a series of docking studies. As shown in Fig. 6, for the most optimal compound **24r**, the binding mode was found to be basically similar to donepezil (Fig. 6B/A). Specifically, one oxygen atom of the

sulfone formed a hydrogen bond (3.0 Å) with Phe295 and the neighboring phenyl ring formed an aromatic π-π stacking interaction (4.0 Å) with residue Trp286. The phenyl ring of the benzylpiperidine moiety bonded with Trp86 of an aromatic π-π stacking interaction (4.3 Å). The charged nitrogen of the piperidine ring formed two π-cation interactions with Phe338 (6.4 Å) and Trp86 (4.5 Å) respectively. The docking results therefore indicate a reasonable explanation for high inhibitory activity of compound **24r**. The activity gap between compounds **12a**(***E***) (*trans*-isomer) and **12a**(***Z***) (*cis*-isomer) might be explained by docking studies (Fig. 6C). The binding mode of compound **12a**(***E***) is similar to donepezil, but the sulfone group of **12a**(***Z***) is completely opposite to the carbonyl group of donepezil, generating the loss of two important π-π stacking interactions with Trp86 and Trp286, resulting in loss of activity. As for compound **24b** (Fig. 6D), it still adopts a similar binding mode with donepezil, so the activity is maintained.

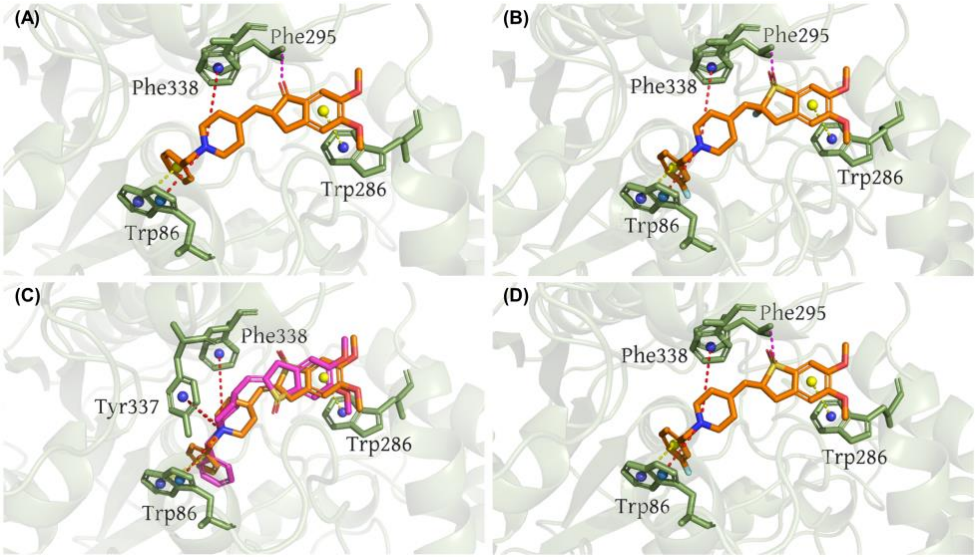

Fig. 6. Proposed binding models of donepezil (A), **24r** (B), **12a**(***E***) and **12a**(***Z***) (C), **24b** (D) with AChE (PDB code: 4EY7). For secondary bonds, hydrogen bonds are shown as magenta dotted lines, π-cation interactions as red dotted lines and π-π stacking interactions as yellow dotted lines. (A) Interactions between donepezil (shown in brown) and key amino acid residues of AChE. (B) Interactions between compound **24r** (shown in brown) and key amino acid residues of AChE. (C) Interactions between compounds **12a**(***E***) (shown in brown) and **12a**(***Z***) (shown in magenta) and key amino acid residues of AChE. (D) Interactions between compound **24b** (shown in brown) and key amino acid residues of AChE.

2.4. In vitro kinetic study of AChE inhibition

To further confirm the mechanism of action of compound **24r**, we conducted a kinetic study on this compound. The linear Lineweaver-Burk plots (1/V *vs.* 1/S) displayed in Fig. 7A showed that as the concentration of inhibitor increased, both slopes and intercepts increased. That means compound **24r** is a mixed-type inhibitor against AChE, and it could bind with both catalytic anionic site (CAS) and peripheral anionic site (PAS) of AChE. Lineweaver-Burk secondary plots were constructed at obtained slope，using the Lineweaver-Burk secondary plots (Fig. 7B), a *K*i value equal to 0.4 nM was obtained for compound **24r**.

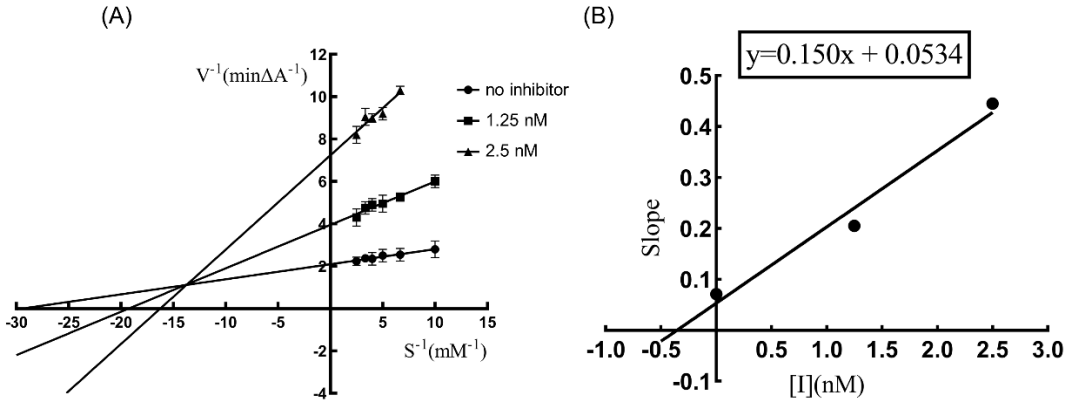

Fig. 7. Kinetic study on the mechanism of compound **24r** inhibiting AChE. (A) Overlaid Lineweaver-Burk reciprocal plots of AChE initial velocity at increasing substrate concentrations (0.10 - 0.40 mM) in the absence of inhibitor and in the presence of **24r** are shown. (B) Lineweaver-Burk secondary plots.

*2.5. Compound **24r** inhibits AChE enzyme in SH-SY5Y differentiated neuronal cells*

Before we started to assess cellular effects of compound **24r** in SH-SY5Y differentiated neuronal cells, we firstly determined its cytotoxicity at a range of concentrations 0.01 μM to 100 μM for compound **24r** and 0.01 μM to 1000 μM for the positive control donepezil using Cell Titer-Glo assay, and found that the maximum non-cytotoxic concentration for compound **24**r or donepezil is 10 μM or 100 μM respectively (data not shown), therefore, testing concentrations below 10 μM for both drugs are used in the following *in vitro* cell based experiments.

In order to assess the efficacy of novel AChE inhibitor **24r**, we determined the AChE inhibitory potency of **24r** and donepezil as reference in SH-SY5Y differentiated neuronal cells using the Ellman assay. As shown in Fig. 8, in the 1 mM glyceraldehyde (GA) exposed neuronal cells we

recorded a significant inhibition of AChE activity by compound **24r** at a concentration as low as 50 nM, with the same trend being scored by the commercial AChE inhibitor donepezil, in a dose dependent manner.

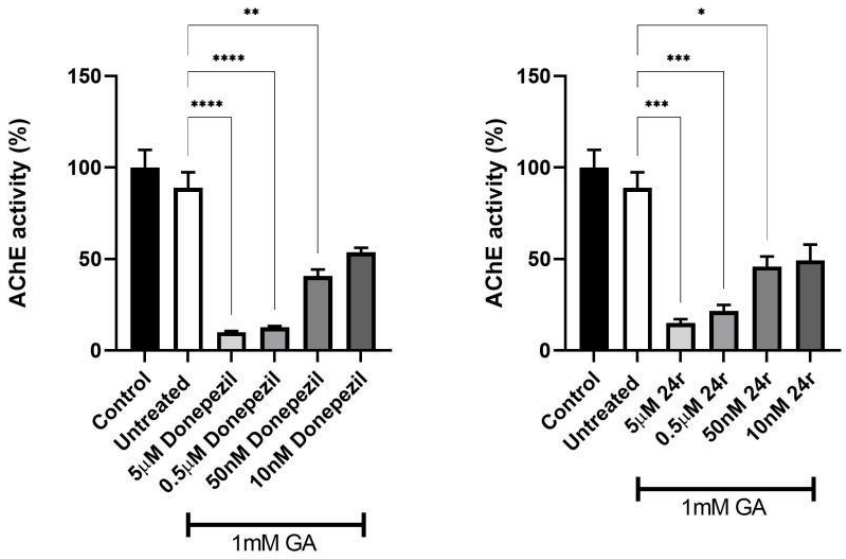

Fig. 8. AChE inhibitory activity in 1 mM GA exposed SH-SY5Y differentiated neuronal cells after donepezil or **24r** treatment at different concentrations. Data are expressed as mean ± SEM (at least n = 3 independent experiments were performed; *$p < 0.05$, **$p < 0.01$, ***$p < 0.001$, ****$p < 0.0001$).

*2.6. Compound **24r** reduces tau phosphorylation at S396 but not at S199*

After validating the inhibitory activity of the novel compound on AChE enzyme, we investigated whether GA-induced tau hyperphosphorylation could be prevented by AChE inhibition exerted by compound **24r**. Exposure of neuronal cells to 1 mM GA dramatically increased tau phosphorylation levels at S199 (Fig. 9A). Compound **24r** and control drug donepezil, did not show a significant reduction of tau phosphorylation at this residue.

To further assess the efficacy of the novel compound in preventing tau abnormal phosphorylation, tau residue S396 was also examined. In neuronal cells treated with 1 mM GA, we recorded an increased phosphorylation level compared to the untreated group. In contrast, the abnormal phosphorylation at tau S396 was significantly reduced by the novel compound **24r** at a

concentration as low as 10 nM, overlapping with the results obtained for the commercially available AChE inhibitor donepezil (Fig. 9B). However, such effect is not dose dependent.

This result is likely caused by the non-specific control of cholinergic signaling over the several kinases and phosphatases involved in tau aberrant phosphorylation. In particular, a link was shown between AChE inhibition and reduction of glycogen synthase kinase-3 (GSK-3) activity, the major tau kinase [38-40]. However, this happens in a non-direct manner, since an increased level of neurotransmitter ACh is present following AChE inhibition, by the activation of M1 receptor, which depletion is as well linked to GSK-3 activation [41, 42].

Thus, the effects observed following treatment with AChE inhibitors strictly depend on the subsequent ACh pathway activation as a result of increased availability of the neurotransmitter, which cannot be controlled by the inhibitor itself.

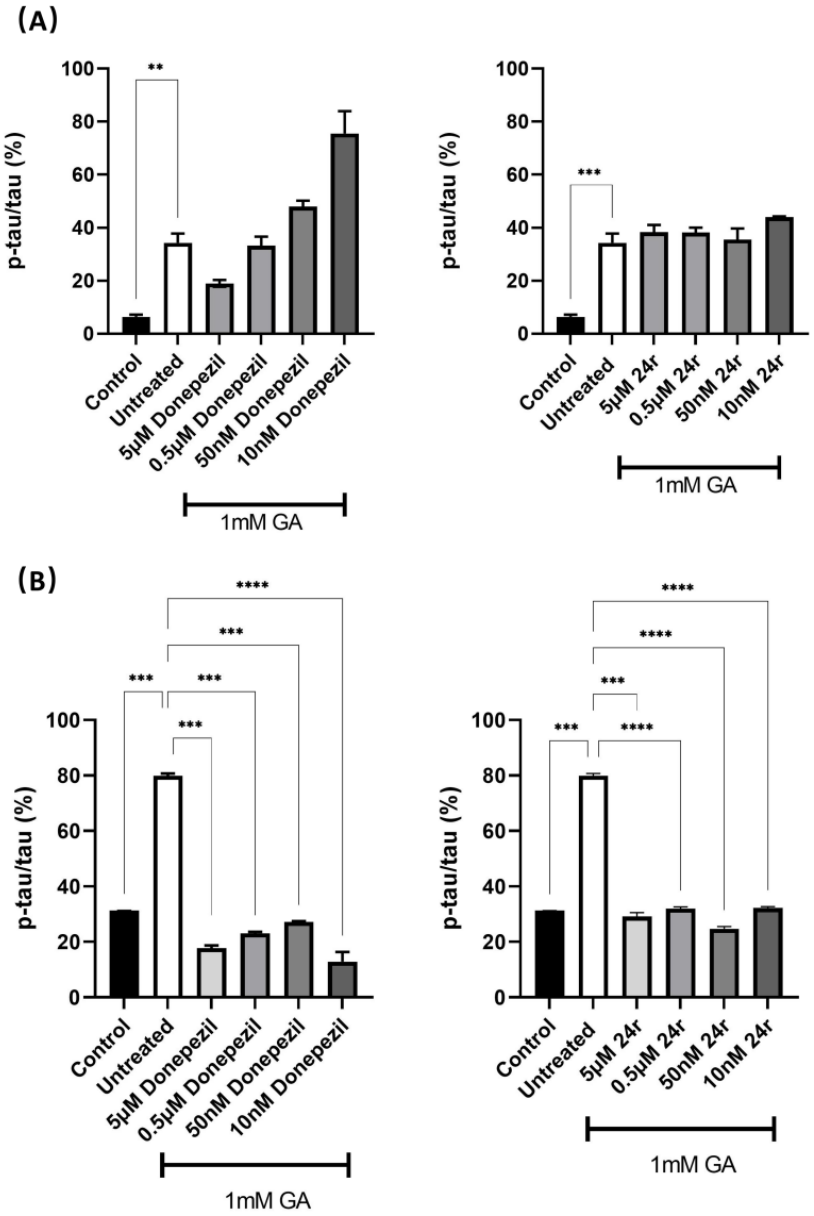

Fig. 9. Quantification of phosphorylation ratio about p-Tau/total tau of GA treated SH-SY5Y differentiated neuronal cells after donepezil or **24r** treatment at different concentrations. Data are expressed as mean ± SEM (at least n = 3 independent experiments were performed; $^{**}p < 0.01$, $^{***}p < 0.001$, $^{****}p < 0.0001$). (A) Phosphorylation results for p-Tau/total tau at S199 site of tau protein after donepezil or **24r** treatment. (B) Phosphorylation results for p-Tau/total tau at S396 site of tau protein after donepezil or **24r** treatment.

*2.7. Compound **24r** provides neuroprotection by rescuing neuronal morphology and increasing cell viability in 1mM GA exposed SH-SY5Y differentiated neuronal cells*

Microtubule architecture plays a fundamental role in cytoskeletal structure in neuronal cells,

assuring a correct morphology and axonal transport. The presence of hyperphosphorylated forms of tau protein leads to a jeopardized microtubule architecture, resulting in a disrupted axon morphology, neurodegeneration, and aberrant axonal transport [43]. As shown in Fig. 10A-C, treatment with GA at 1 mM concentration resulted in a dramatic increase in tau phosphorylation levels, which led to morphology defects and neurite shortening.

To assess whether the novel AChE inhibitor is able to prevent the formation of morphological defects in GA treated neuronal cells and further provide neuroprotection, confocal microscopy is used to image neuronal cells treated with either 5 μM or 0.5 μM of the novel therapy in comparison with donepezil. Treatment with compound **24r** resulted in increased axon length and prevented the formation of morphological defects at both concentrations investigated (Fig. 10C). Conversely, donepezil was able to replicate compound **24r** results only when administrated at 0.5 μM, while a higher non-cytotoxic concentration of 5 μM showed no preventive effect on neuronal morphology as to a similar extent as untreated (Fig. 10B), although at such concentration donepezil increased cell viability (Fig. 10D). The mechanism underlining this phenomenon would require further investigation.

In addition to compromised neuronal morphology, depletion of cholinergic neuronal cells is a well-known characteristic of AD pathogenesis, with the major circuits involved in memory and learning functions represented by this type of neuronal cells. In order to study whether inhibition of AChE would result in an increased cell viability after 1 mM GA treatment a Methylthiazolyldiphenyl-tetrazolium bromide (MTT) assay was performed. In neuronal cells treated with 1 mM GA, compound **24r** treatment significantly prevented the dramatic cell death observed in untreated neuronal cells when administrated at 0.5 μM, and showed a similar amelioration but with statistical insignificance when administrated at 5 μM (Fig. 10E). On the other hand, the control drug donepezil successfully increased cell viability at both concentrations tested (Fig. 10D), despite no effect observed on neuronal morphology at a higher concentration of 5 μM (Fig. 10B).

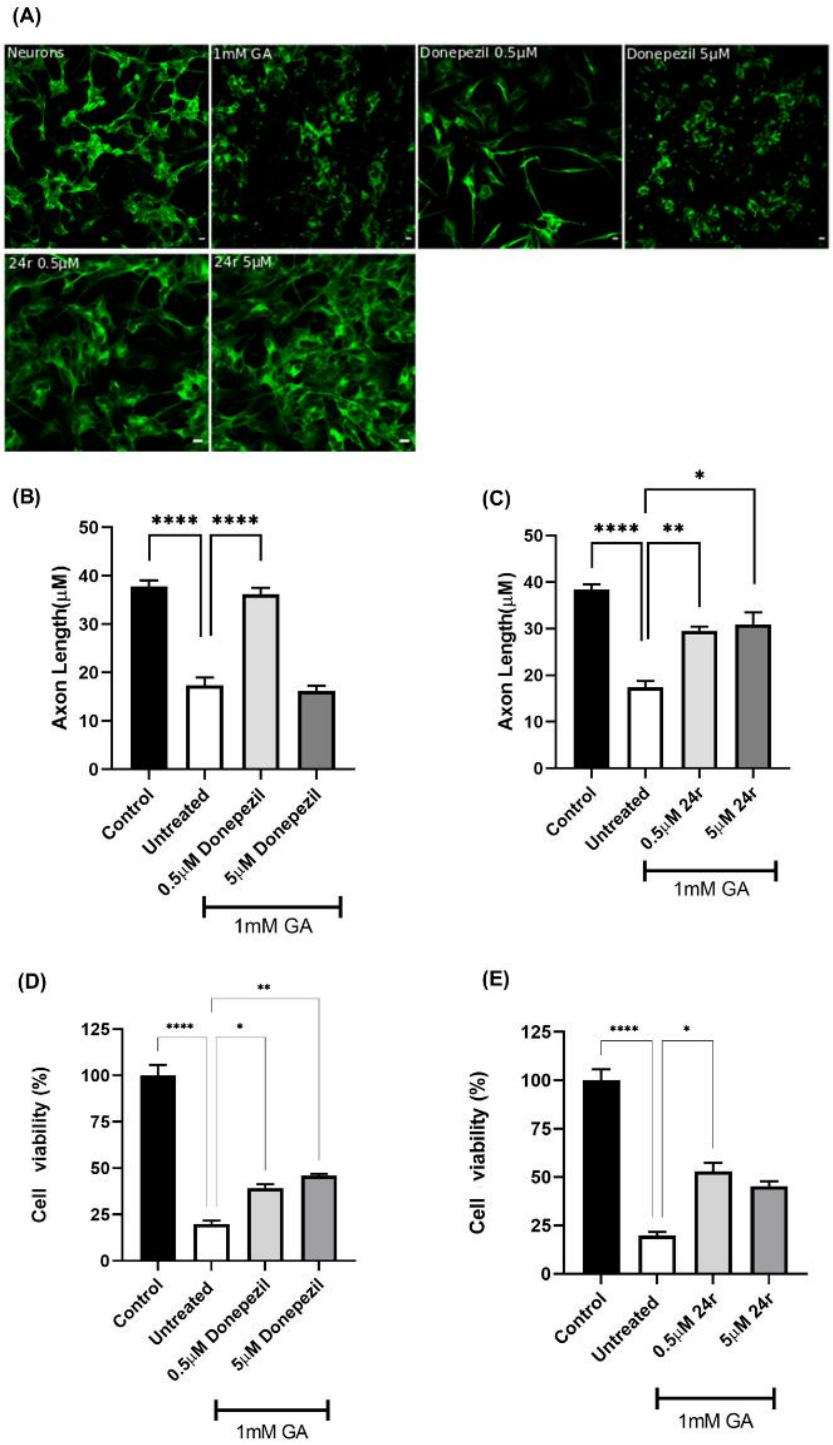

Fig. 10. Neuron-like morphology and cell viability in 1 mM GA exposed SH-SY5Y differentiated neuronal cells after donepezil or **24r** treatment at different concentrations. Data are expressed as mean ± SEM (at least n = 3 independent experiments were performed; *$p < 0.05$, **$p < 0.01$, ****$p < 0.0001$). (A) Confocal image of GA treated SH-SY5Y differentiated neuronal cells after donepezil or **24r** treatment at different concentrations. (B-C) Axon length in SH-SY5Y differentiated neuronal cells after treatment of donepezil or **24r**. (D-E) Cell viability of SH-SY5Y differentiated neuronal cells after donepezil or **24r** treatment at different concentrations, using an MTT assay.

*2.8. Compound **24r** reduces amyloid aggregation in presence of AChE enzyme*

Tau hyperphosphorylation and deposition of amyloid plaques are considered to be the two major players in AD pathogenesis [44]. Since AChE has a function in promoting β-amyloid peptide aggregation, we investigated whether the novel compound could decrease the aggregation rate by binding to AChE enzyme. Compound **24r** treatment supported the theory that inhibition of AChE enzyme results in a reduction in β-peptide aggregation rate, with all concentrations investigated resulting in a significant drop (Fig. 11). Similar results were obtained with donepezil, which significantly reduced the amyloid aggregation rate at all concentrations studied.

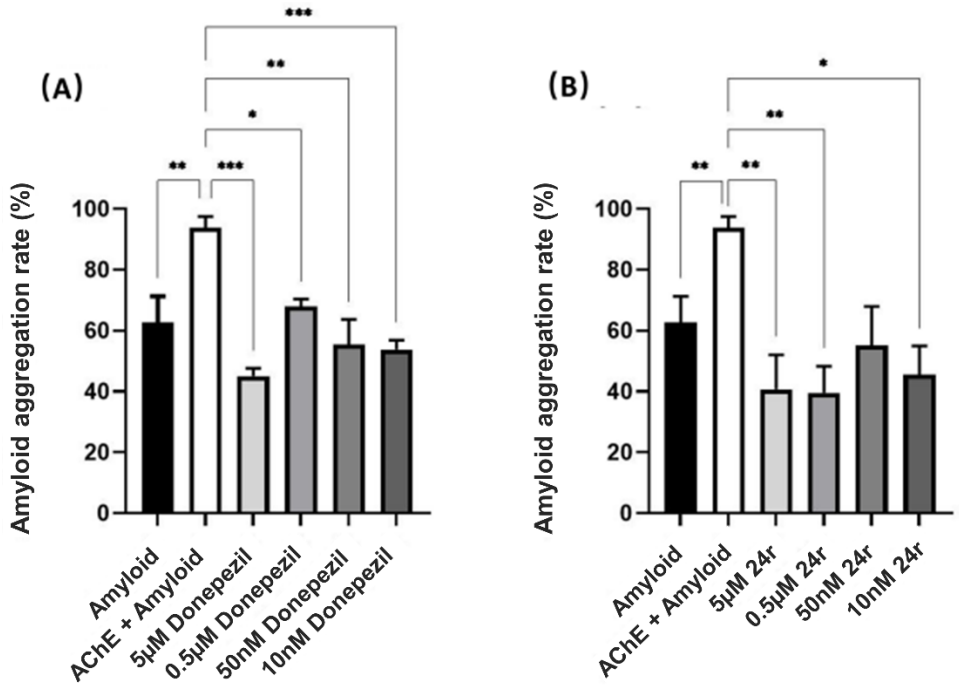

Fig. 11. Amyloid aggregation in presence of AChE enzyme after donepezil (A) or **24r** (B) treatment at different concentrations. Data are expressed as mean ± SEM (at least n = 3 independent experiments were performed; *p < 0.05, **p < 0.01, ***p < 0.001).

*2.9. Compound **24r** protects against okadaic acid induced mitochondrial dysfunction*

Mitochondrial dysfunction has been identified in a large proportion of neurodegenerative diseases and it is a key factor in okadaic acid-induced memory impairment and cell death in rodent models used to study AD [45]. Prior studies have shown that mitochondrial dysfunction and memory

impairment can be prevented by donepezil treatment [45].

To investigate whether compound **24r** protects against okadaic-acid induced mitochondrial dysfunction we explored mitochondrial membrane potential (MMP) in SH-SY5Y cells using the 5,5',6,6'-tetrachloro-1,1',3,3'-tetraethyl-benzimidazol-carbocyanine iodide (JC-1) fluorescent cell-based assay. JC-1 aggregates in healthy mitochondria and has a red fluorescence, whereas its monomeric form has a green fluorescence. Thus, the red/green fluorescence intensity ratio is a measurement of mitochondrial function.

As shown in Fig. 12A, treatment with okadaic acid enhanced green fluorescence and reduced red fluorescence, causing a reduction in the red/green fluorescence intensity ratio compared to the control. Pre-treatment of SH-SY5Y cells for 24 hours with compound **24r** (5 μM and 0.5 μM) and donepezil (5 μM and 0.5 μM) reduced the effects of okadaic acid on the MMP, indicating a protective effect of these compounds ($P < 0.05$, *vs.* vehicle + okadaic acid). Overall compound **24r** has stronger protection than donepezil, both in a dose dependent manner.

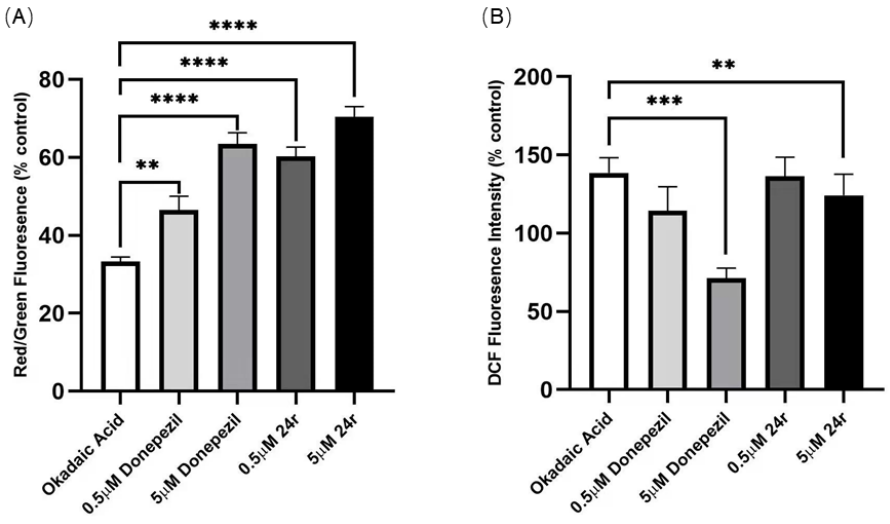

Fig. 12. Compound **24r** showed effective performance in two okadaic acid-induced pharmacological models. SH-SY5Y cells were treated for 24 h with increasing concentrations of test compound **24r** and positive control donepezil (5 μM - 0.5 μM) prior to exposure to 0.03 μM okadaic acid for an additional 24 h. Data are expressed as mean ± SEM (at least n = 3 independent experiments were performed; $^{**}P < 0.01$, $^{***}P < 0.001$, $^{****}P < 0.0001$). (A) Ratio of red to green fluorescence following JC-1 assay in the culture of SH-SY5Y cells. (B) DCF fluorescence intensity in the culture of SH-SY5Y cells.

*2.10. Compound **24r** protects against okadaic acid induced ROS*

With a deepening understanding of cellular mechanisms, oxidative stress is considered as one of the causes of AD [46]. To explore the possibility that compound **24r** would protect against okadaic acid-induced reactive oxygen species (ROS) generation, we measured intracellular ROS levels using the 2',7'-Dichlorofluorescin diacetate (DCFH-DA) fluorescence assay. Within the cell, DCFH-DA is converted to nonfluorescent 2',7'-Dichlorofluorescin (DCF) which is then oxidized to fluorescent DCF in the presence of ROS. The green fluorescence intensity as a result of this reaction measures intracellular ROS levels.

Treatment of SH-SY5Y cells with 0.03 μM okadaic acid increased DCF fluorescence compared to non-treated cells. Pre-treatment of these cells with donepezil and compound **24r** both reduced DCF fluorescence intensity at the concentration of 5 μM, but not 0.5 μM as shown in Fig. 12B. These results therefore demonstrate that okadaic acid induces ROS generation, and compound **24r** can effectively protect against this effect, preventing the generation of intracellular ROS at 5 μM ($P < 0.05$, *vs.* vehicle + okadaic acid), with a similar profile as donepezil.

2.11. Cytochrome P450s inhibition assay

Inspired by the excellent *in vitro* inhibitory potency of compound **24r**, we subsequently prepared compound **24r** hydrochloride (**24r-HCl**) to perform subsequent evaluation. Cytochrome P450s (CYPs) represent a superfamily of enzymes that catalyze the oxidation of a wide variety of drugs. Drug-drug interactions (DDI) caused by inhibiting CYP450s enzymes may lead to dangerous and serious side effects [47]. We investigated the effect of compound **24r-HCl** on a panel of CYP isoforms (CYP2C9, CYP2D6, CYP3A4-M (midazolam as substrate) and CYP3A4-T (testosterone as substrate)) in human liver microsomes (HLMs). As shown in Table 4, compound **24r-HCl** showed weak inhibition against CYP2C9, CYP2D6, CYP3A4-M and CYP3A4-T with IC_{50} values of > 20 μM, indicating that compound **24r-HCl** presents low potential to cause DDI in metabolic pathways.

Table 4. *In vitro* CYP inhibition assessment of compound **24r-HCl**. [a]

Compd.	IC_{50} values of CYP isoforms (μM)			
	CYP2C9	CYP2D6	CYP3A4-M	CYP3A4-T
24r-HCl	>20	>20	>20	>20

[a] Assays were performed in pooled human liver microsomes.

2.12. In vivo blood-brain barrier permeability

Blood-brain barrier (BBB) permeability is a basic requirement for successful drug delivery to the central nervous system, especially for anti-AD drugs. Therefore, we next carried out an *in vivo* assay with Institute of Cancer Research (ICR) mice to evaluate the permeability of compound **24r** to the BBB. The results are presented in Table 5. After intragastric administration (i.g.) at the dosage of 1 mg/kg, compound **24r** could be easily detected in both plasma and brain. Specifically, the concentration of compound **24r** in plasma increased slightly from 2.89 to 3.48 ng/mL (from 0.25 h to 1 h) and then gradually decreased from 3.48 to 2.70 ng/mL (from 1 h to 4 h). In contrast, the concentration of compound **24r** in brain increased obviously from 10.58 to 21.95 ng/mL (from 0.25 h to 1 h) and remained unchanged until 4 h. Meanwhile, the ratio of brain/plasma of compound **24r** remained between 4.167 and 8.467 at all timepoints. Thus, the results of this assay indicated that compound **24r** possessed the excellent ability to penetrate the BBB, which might be due to the successful introduction of fluorine atoms.

Table 5. The concentration of compound **24r** in plasma, brain and ratio of brain/plasma after i.g. administration (1 mg/kg) [a].

T (h)	Concentration of **24r**		Ratio of Brain/Plasma
	Plasma (ng/mL)	Brain (ng/mL)	
0.25	2.89 ± 2.26	10.58 ± 6.53	**4.167** ± 0.967
0.5	3.42 ± 0.31	18.07 ± 3.68	**5.240** ± 0.584
1	3.48± 0.33	21.95 ± 1.34	**6.325** ± 0.219
2	2.59 ± 0.09	21.83 ± 3.78	**8.397** ± 1.180

4	2.70 ± 1.14	21.70 ± 5.51	**8.467** ± 1.813

[a] Values are expressed as the mean ± SD (n = 3).

2.13. In vivo inhibitory activity against AChE

Compound **24r-HCl** was performed an evaluation of AChE inhibition *in vivo*, to assess a dose-dependent effect, mice were treated by i.g. administration with compounds **24r-HCl** (0.5, 1, 2, 4 mg/kg) and donepezil (10 mg/kg) as a positive control, then AChE activity in the cortex and hippocampus were tested after 1 h. The results are shown in Fig. 13. At a dosage of 1, 2, 4 mg/kg, compound **24r-HCl** significantly inhibited the AChE activity in the cortex and hippocampus in a dose-dependent manner, and the inhibitory activity at a dosage of 4 mg/kg of compound **24r-HCl** was more potent than that of donepezil at a dose of 10 mg/kg. This preliminary result indicated that compound **24r** is able to well penetrate the BBB and inhibit AChE in the brain to the similar extent at less than a half dosage (4 mg/kg) than donepezil (10 mg/kg).

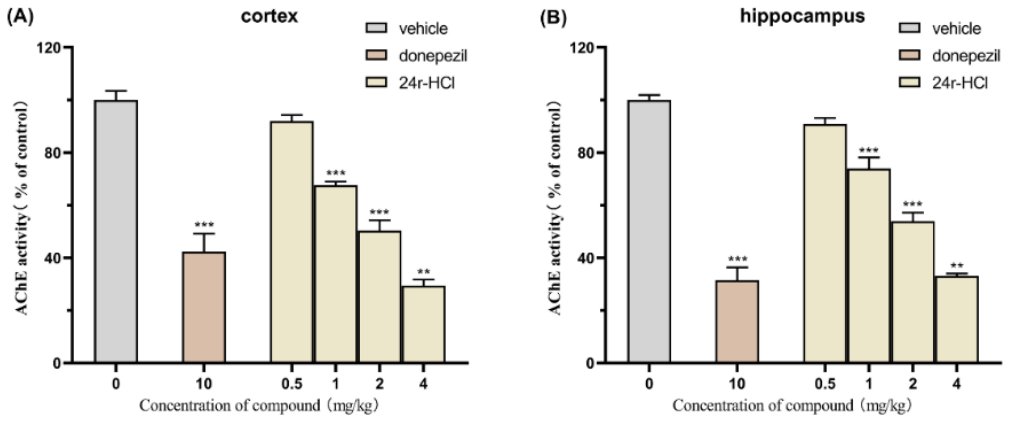

Fig. 13. *In vivo* inhibitory activities against AChE of compound **24r-HCl** (i.g.) in the cortex (A) and hippocampus (B) of ICR mice. Data were represented as the percentage of vehicle control mice; they were set to 100% and presented as mean ± SEM (n = 4). $^{**}P < 0.01$, $^{***}P < 0.001$ *vs.* the control group.

2.14. In vivo behavioral studies in scopolamine-induced cognition-impaired mice

Inspired by excellent evaluation results of compound **24r** above, we performed a step-through passive avoidance test to evaluate the ability of compound **24r** to improve memory impairment using scopolamine-induced cognition-impaired ICR mice and donepezil hydrochloride was used as

a positive control [48, 49].

A total of 120 female ICR adult mice were randomly divided into six groups, with 20 mice per group: control group, model group (scopolamine), positive control group (5 mg/kg donepezil hydrochloride), low dosage group (0.1 mg/kg **24r-HCl**), medium dosage group (0.3 mg/kg **24r-HCl**) and high dosage group (1 mg/kg **24r-HCl**). Three separate trials were performed on all mice after i.g. administration: a training trial, a learning trial and a memory trial. The latency time and the number of errors in the learning trial and memory trial of mice were recorded and the results are shown in Fig. 14. In the learning trial, there was no statistical difference in the latency time between the groups (P = 0.212), but there was a statistical difference in the number of errors; the number of errors in the control group was significantly reduced (P = 0.0038) compared with the model group. In the memory trial, the latency time of the mice in the control group (195.20 s) was significantly increased (P = 0.0003), and the number of errors of the mice in the control group (0.74) was decreased compared with the model group (65.40 s, 2.95). Meanwhile, the number of errors in the donepezil group (1.95), the low dose group (1.60) and the medium dose group (1.70) were significantly decreased. Collectively, the results indicated that compound **24r-HCl** at 0.1 mg/kg or 0.3 mg/kg was able to significantly improve the memory impairment of mice induced by scopolamine, and the lowest dosage of 0.1 mg/kg was better than 5 mg/kg of donepezil. Thus, the results of step-through passive avoidance test demonstrated that compound **24r** is able to reverse cognitive deficit at a fifty times lower concentration (0.1 mg/kg) than donepezil (5 mg/kg).

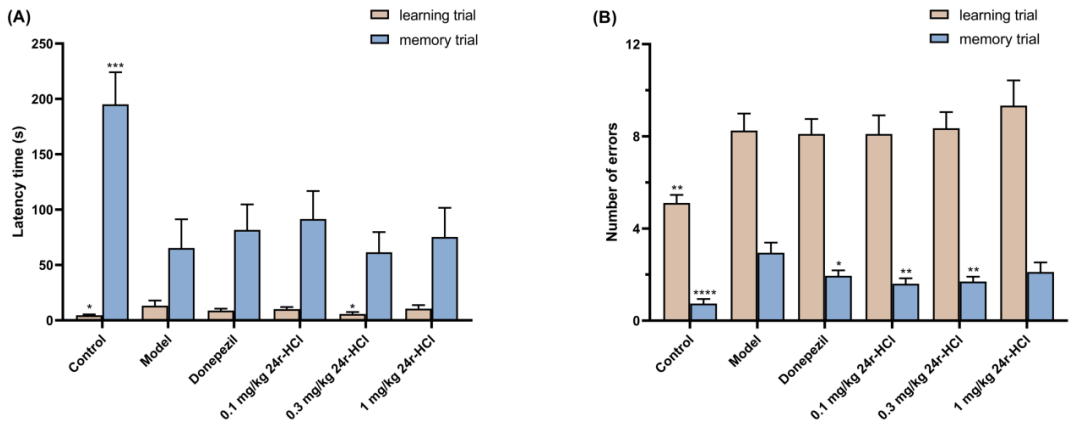

Fig. 14. Effects of compound **24r-HCl** on the (A) latency time (s) and (B) number of errors in the step-through test by the scopolamine-induced cognitive deficit. Values are expressed as the mean ± SEM (n = 18 - 20). *P < 0.05,

$^{**}P < 0.01$, $^{***}P < 0.001$, $^{****}P < 0.0001$ *vs.* model group.

3. Conclusions

In conclusion, for the first time, we successfully introduced alkenyl sulfone and sulfone moieties, a class of fragments with neuroprotective functions, into the structure of parent compound donepezil. After three series of structural optimization, we identified the most potent compound **24r** bearing strong AChE inhibitory potency (IC_{50} = 2.4 nM) *in vitro*. Kinetic and docking studies indicated that compound **24r** was a mixed-type inhibitor and bonded with CAS and PAS of AChE simultaneously.

In the follow-up pharmacological evaluations, compound **24r** did not only inhibit AChE in SH-SY5Y differentiated neuronal cells, it also reduced GA-induced phosphorylation of the tau protein at its residue S396 but not at S199 residue, indicating that compound **24r** may influence the regulation of the tau protein signaling pathway via GSK-3 kinase. Meanwhile, compound **24r** could provide neuroprotection by rescuing neuronal morphology and increasing cell viability in 1mM GA exposed SH-SY5Y differentiated neuronal cells, while donepezil had no such effect at a high concentration even though cell viability was increased. Besides, compound **24r** could also reduce amyloid aggregation to highlight the possibility of a synergistic treatment effect for AD. Moreover, compound **24r** was found to be more effective than donepezil in two okadaic acid-induced pharmacological models, it is more potent to protect from mitochondrial dysfunction, and provide protection against ROS generation from the neurotoxic effects induced by okadaic acid. Importantly, the BBB permeability and *in vivo* AChE inhibitory activity showed that compound **24r** could penetrate BBB well and inhibit AChE activity in the brain to the same extent at a dose of 2 times lower than donepezil. The behavioral studies of compound **24r** on scopolamine-induced cognition-impaired mice strongly suggested that compound **24r** could significantly improve the learning and memory impairment of mice at a dose of 50 times lower than donepezil.

In summary, the novel AChE inhibitor **24r** exhibits more potent activity of the enzymatic inhibition and a better neuroprotective profile than donepezil, as well as good improvement in learning and memory impairment of mice at a much lower dose than donepezil. In addition, compound **24r** shows the potential to treat AD through additional processes, such as the inhibition

of tau phosphorylation and amyloid aggregation, neuroprotection, anti-oxidation and protection from mitochondrial dysfunction. Thus, compound **24r** is a promising lead compound for the further investigation to discovery and development of new anti-AD agents.

4. Experimental section

4.1. Chemistry

All reagents were chemically pure or analytical pure products purchased from Energy Chemical (China) or Bidepharm (China) and used without further purification. Anhydrous dichloromethane (DCM) was dried with phosphorus pentoxide (P_2O_5) and then distilled; anhydrous *N*, *N*-dimethylformamide (DMF) was pretreated with anhydrous magnesium sulfate ($MgSO_4$), and then treated with calcium hydride (CaH_2) and distilled under in vacuum; Anhydrous tetrahydrofuran (THF) was obtained by refluxing with sodium (Na) until the benzophenone getting blue and then distilled; the remaining solvents were used directly without treatment unless otherwise specified. Flash column chromatography was performed on 200-300 mesh silica gel (Qingdao Haiyang Chemical, China). Reactions were monitored by thin-layer chromatography (TLC) on 0.25 mm silica gel GF254 plates and visualized under UV light (λ = 254 nm). ^{1}H NMR and ^{13}C NMR spectra were recorded by a Bruker Advance 400 or 300 MHz (Bruker Company, Germany) in the indicated solvents ($CDCl_3$ or DMSO-d_6) and with tetramethylsilane (TMS) as an internal standard. Chemical shifts were reported in ppm (δ) values and the coupling constants (J) in Hz. Proton coupling patterns were described as singlet (s), broad singlet (brs), doublet (d), doublet of doublets (dd), triplet (t), quartet (q) and multiplet (m). The high-resolution mass spectrometry (HRMS) was measured on a Finnigan MAT 95 spectrometer (Finnigan, Germany). The purity of representative compounds was $\geqslant$ 98%, as estimated by HPLC (SHIMADZU Lab solutions, UV detection at λ = 254 nm) analysis on the Aglilent C_{18} column (4.6 $\times$ 150 mm, 5 μm) eluting at 1 mL/min of menthol and water (80:20).

*4.1.1. Synthesis of compound **2a***

Phthyl ether (21 g, 156 mmol) was dissolved in DCM (50 mL), and chlorosulfonic acid (30 mL, 469 mmol) was slowly added under ice bath. Then thionyl chloride (11 mL, 156 mmol) was slowly

added. After the reaction was stirred at room temperature for 1 h, quenched with water, extracted with DCM (50 mL × 3). The combined organic layers were washed with saturated brine, dried over anhydrous Na_2SO_4. The solvent was evaporated under a vacuum to obtain compound **2a** (33.6 g, 142.0 mmol, 93% yield), which were used for the next step directly.

*4.1.2. Synthesis of compound **3a***

Zinc (46 g, 709.1 mmol) was added to a solution of compound **2a** (33.6 g, 142.0 mmol) in EA (100 mL), and concentrated hydrochloric acid (130 mL, 1.56 mol) was slowly added dropwise. After the reaction was stirred at room temperature for 2 h, the zinc was removed by filtration, the solvent was extracted with EA (100 mL×3) and the combined organic layers were washed with saturated brine, dried over anhydrous Na_2SO_4. The solvent was evaporated under a vacuum to obtain compound **3a** (20.5g, 120.4 mmol, 85% yield), which were used for the next step directly.

*4.1.3. Synthesis of compounds **4a-c***

K_2CO_3 (6.8 g, 49.4 mmol) was added to a solution of compound **3a** (5.6 g, 32.90 mmol) in CH_3CN (50 mL) and the reaction was stirred for 10 minutes. diethyl *p*-toluenesulfonyloxymethylphosphonate (13.8 g, 42.77 mmol) was added and stirred at 50 ℃ for 2 h. The reaction mixture was concentrated *in vacuo*, diluted with H_2O, extracted with DCM (50 mL × 3) then washed with brine, dried over anhydrous Na_2SO_4. The solvent was evaporated under a vacuum, and the crude products were purified by column chromatography (DCM/CH_3OH, 200:1, v/v) to obtain compound **4a** (6.6 g, 20.6 mmol, 63% yield).

NCS (871 mg, 6.52 mmol) was added to a solution of compound **4a** (1.90 g, 5.93 mmol) in CCl_4 (20 mL), and the reaction was stirred at room temperature for 2 h. The reaction solution was filtered and the filtrate was concentrated *in vacuo*. Then the crude products were purified by column chromatography (DCM/CH_3OH, 200:1, v/v) to obtained compound **4b** (1.52 g, 4.28 mmol, 72% yield). Compound **4b** (500 mg, 1.41 mmol) was dissolved in methanol (10 mL), and the reaction was refluxed for 0.5 h. The methanol was evaporated and the crude products were purified by column chromatography (DCM/CH_3OH, 200:1, v/v) to obtained under a vacuum to obtain compound **4c** (443 mg, 1.26 mmol, 90% yield).

*4.1.4. Synthesis of compounds **6a-c***

m-CPBA (1.10 mmol) was added to a solution of compounds **4a-c** (0.50 mmol) in DCM. After the reaction was stirred at room temperature for 2 h, quenched with $Na_2S_2O_3$, extracted with DCM (20 mL × 3). The combined organic layers were washed with saturated $NaHCO_3$, brine, and dried over anhydrous Na_2SO_4. The solvent was evaporated under a vacuum, the crude product was purified by column chromatography (DCM/CH_3OH, 100:1, v/v) to obtain intermediates **5a-c** with yields of 78% - 91%. Then, NaH (0.38 mmol) was added to a solution of **5a-c** (0.32 mmol) in dry THF degasified with N_2 under an ice bath, the resulting solution was stirred for 0.5 h, 1-benzylpiperidine-4-carbaldehyde (0.42 mmol) was added. The reaction was stirred at room temperature for 5 h. The reaction was quenched with H_2O, extracted with DCM (20 mL × 3), the combined organic layers were washed with brine, dried over anhydrous Na_2SO_4. The solvent was evaporated under a vacuum, and the crude products were purified by column chromatography (DCM/CH_3OH, 30:1, v/v) to obtain intermediates **6a-c** with yields of 44% - 87%.

*(E)-1-benzyl-4-(2-((3,4-dimethoxyphenyl)sulfonyl)vinyl)piperidine (**6a**)*. Yellow solid, 87% yield. ^{1}H NMR (300 MHz, Chloroform-*d*) δ 7.48 (dd, *J* = 8.5, 2.1 Hz, 1H), 7.29 (d, *J* = 3.6 Hz, 6H), 6.99 – 6.85 (m, 2H), 6.26 (dd, *J* = 15.1, 1.5 Hz, 1H), 3.93 (d, *J* = 6.0 Hz, 6H), 3.48 (s, 2H), 2.89 (dt, *J* = 12.2, 3.4 Hz, 2H), 2.24 – 2.12 (m, 1H), 1.98 (td, *J* = 11.8, 2.4 Hz, 2H), 1.71 (d, *J* = 12.8 Hz, 2H), 1.47 (tt, *J* = 11.9, 6.0 Hz, 2H). ^{13}C NMR (75 MHz, Chloroform-*d*) δ 153.08, 149.23, 149.20, 138.23, 132.17, 129.44, 129.08, 128.22, 127.04, 121.73, 110.84, 109.74, 63.21, 56.26, 52.99, 38.00, 30.58. HR-MS (ESI) m/z: calcd for $C_{22}H_{28}NO_4S$ $[M+H]^+$ 402.1734, found 402.1739.

*(Z)-1-benzyl-4-(2-chloro-2-((3,4-dimethoxyphenyl)sulfonyl)vinyl)piperidine (**6b**)*. Yellow solid, 58% yield. ^{1}H NMR (300 MHz, Chloroform-*d*) δ 7.54 (dd, *J* = 8.5, 2.2 Hz, 1H), 7.39 – 7.26 (m, 6H), 7.03 (d, *J* = 9.3 Hz, 1H), 6.97 (d, *J* = 8.6 Hz, 1H), 3.96 (s, 3H), 3.93 (s, 3H), 3.50 (s, 2H), 2.95 – 2.82 (m, 2H), 2.55 – 2.39 (m, 1H), 2.15 – 1.96 (m, 2H), 1.76 – 1.49 (m, 4H). ^{13}C NMR (75 MHz, Chloroform-*d*) δ 153.77, 149.16, 146.69, 142.63, 138.08, 132.14, 129.23, 129.15, 128.25, 127.09, 123.42, 122.89, 110.93, 110.70, 63.34, 56.32, 56.28, 52.68, 36.50, 30.18. HR-MS (ESI) m/z: calcd for $C_{22}H_{27}ClNO_4S$ $[M+H]^+$ 436.1344, found 436.1350.

*(E)-1-benzyl-4-(2-((3,4-dimethoxyphenyl)sulfonyl)-2-methoxyvinyl)piperidine (**6c**)*. Yellow solid, 44% yield. ^{1}H NMR (300 MHz, Chloroform-*d*) δ 7.52 (dd, *J* = 8.5, 2.1 Hz, 1H), 7.37 – 7.26 (m, 6H), 6.96 (d, *J* = 8.5 Hz, 1H), 6.28 (d, *J* = 10.0 Hz, 1H), 3.94 (s, 3H), 3.92 (s, 3H), 3.82 (s, 3H), 3.50 (s, 2H), 2.88 (dt, *J* = 11.9, 3.5 Hz, 2H), 2.42 (ddq, *J* = 15.0, 10.3, 4.4 Hz, 1H), 2.01 (td, *J* = 11.4, 3.0 Hz, 2H), 1.68 – 1.49 (m, 4H). ^{13}C NMR (75 MHz, Chloroform-*d*) δ 153.33, 153.22, 149.11, 138.10, 130.37, 130.06, 129.17, 128.23, 127.07, 122.56, 110.69, 110.33, 63.75, 63.38, 56.25, 56.22, 52.87, 33.52, 31.44. HR-MS (ESI) m/z: calcd for $C_{23}H_{30}NO_5S$ $[M+H]^+$ 432.1839, found 432.1841.

*4.1.5. Synthesis of compound **4d***

K_2CO_3 (6.42 g, 46.52 mmol) was added to a solution of compound **3a** (6.60 g, 38.77 mmol) in anhydrous CH_3CN (30 mL), and ethyl bromoacetate (7.77 g, 46.53 mmol) was added dropwise. After the reaction was stirred at room temperature for 3 h, the reaction mixture was concentrated *in vacuo*, extracted with DCM (50 mL × 3), then the combined organic layers were washed with brine, and dried over anhydrous Na_2SO_4. The solvent was evaporated under a vacuum, then the crude products were purified by column chromatography (PE/EA, 4:1, v/v) to obtain compound **4d** (9.14 g, 35.66 mmol, 92% yield).

*4.1.6. Synthesis of compound **5d***

Similar to the reaction procedures for compounds **5a-c**, *m*-CPBA (741 mg, 4.29 mmol) was added to a solution of compound **4d** (500 mg, 1.95 mmol) in DCM. The reaction was stirred at room temperature for 2 h. After a usual workup, the crude products were purified by column chromatography (PE/EA, 2:1, v/v) to obtain compound **5d** (460 mg, 1.60 mmol, 82% yield).

*4.1.7. Synthesis of compound **6d***

Two drops of piperidine and two drops of acetic acid were added to a solution of compound **5d** (150 mg, 0.52 mmol) in toluene (10 mL), and 1-benzylpiperidine-4-carbaldehyde (127 mg, 0.62 mmol) was added. After the reaction was refluxed for 12 h, then the reaction mixture was concentrated *in vacuo*. The crude products were purified by column chromatography (DCM/CH_3OH, 30:1, v/v) to obtain compound **6d** (86 mg, 0.18 mmol, 35% yield).

*Ethyl (E)-3-(1-benzylpiperidin-4-yl)-2-((3,4-dimethoxyphenyl)sulfonyl)acrylate (**6d**)*. Yellow oil, 35% yield. ^{1}H NMR (400 MHz, Chloroform-*d*) δ 7.46 (dd, *J* = 8.5, 2.2 Hz, 1H), 7.34 – 7.27 (m, 5H), 6.96 (d, *J* = 8.5 Hz, 1H), 5.29 (d, *J* = 10.3 Hz, 1H), 4.79 (d, *J* = 10.4 Hz, 1H), 4.21 (qd, *J* = 7.1, 2.2 Hz, 2H), 3.97 (s, 3H), 3.91 (s, 3H), 3.48 (d, *J* = 2.5 Hz, 2H), 2.53 – 2.46 (m, 1H), 2.39 (ddt, *J* = 13.1, 6.3, 3.8 Hz, 2H), 2.26 (p, *J* = 6.1 Hz, 4H), 2.14 (d, *J* = 5.9 Hz, 2H), 1.26 (s, 3H). ^{13}C NMR (101 MHz, Chloroform-*d*) δ 165.24, 153.79, 148.85, 147.73, 137.91, 129.15, 128.66, 128.27, 127.18, 123.99, 111.75, 110.38, 110.25, 69.53, 62.67, 62.44, 56.30, 54.43, 53.57, 36.08, 13.99. HR-MS (ESI) m/z: calcd for $C_{25}H_{32}NO_5S$ $[M+H]^+$ 474.1945, found 474.1949.

*4.1.8. General Procedure for Synthesis of compounds **8a-c***

K_2CO_3 (6.4 g, 46.5 mmol) was added to a solution of compound **3a** (6.6 g, 38.8 mmol) in anhydrous CH_3CN (30 mL), and the bromide (46.5 mmol) was added dropwise. After the reaction was stirred at room temperature for 3 h, the reaction mixture was concentrated *in vacuo*, extracted with DCM (50 mL × 3), then the combined organic layers were washed with brine, and dried over anhydrous Na_2SO_4. The solvent was evaporated under a vacuum, then the crude products (**7a-c**) were dissolved in CH_3OH (30 mL), NaOH (30 mL, 10%) was added and stirred at 80 ℃ for 1 h. The reaction mixture was concentrated under a vacuum, neutralized with HCl (1 mol/L) to adjust the pH to 3.0. Then the mixture was filtered and the filtrate was washed with water to obtain intermediates **8a-c** with yields of 88% - 92%.

*4.1.9. General Procedure for Synthesis of compounds **9a-c***

One drop of pyridine was added to a solution of intermediates **8a-c** (8.8 mmol) in DCM (60 mL), oxalyl chloride (2.2 mL, 26.3 mmol) was added dropwise slowly under an ice bath and the reaction was stirred at room temperature for 1 h. The solvent and excess oxalyl chloride were removed *in vacuo*. The resulting crude products were dissolved in dry DCM (60 mL), $AlCl_3$ (1.2 g, 9.2 mmol) was added into the solution under an ice bath. The reaction was stirred at room temperature for 8 h, extracted with DCM (50 mL × 3). The combined organic layers were washed with brine, dried over anhydrous Na_2SO_4. The solvent was evaporated under a vacuum, and the crude products were recrystallized to obtain intermediates **9a-c** with yields of 64% - 73%.

*4.1.10. General Procedure for Synthesis of compounds **11a-c***

$(CH_3CH_2)_3SI$ (0.15 mL) was added to a solution of intermediates **9a-c** (0.95 mmol) in TFA (20 mL) and the reaction was refluxed for 48 h. The reaction mixture was concentrated *in vacuo*, extracted with DCM (50 mL × 3), the combined organic layers were washed with brine, and dried with anhydrous Na_2SO_4. The solvent was evaporated under a vacuum to obtain the crude products (**10a-c**, yields: 58% - 66%). Then similar to the reaction procedures for compounds **5a-c**, the crude products (**10a-c**, 0.51 mmol) were dissolved in DCM, *m*-CPBA (2.09 mmol) was added and the reaction was stirred at room temperature for 2 h. After a usual workup, the crude products were purified by column chromatography (PE/EA, 2:1, v/v) to obtain intermediates **11a-c** with yields of 75% - 89%.

*4.1.11. General Procedure for Synthesis of compounds **12a(Z)**, **12a(E)**, **12b** and **12c***

Compounds **11a-c** (0.22 mmol) was dissolved in anhydrous THF and the solution was degasified with N_2, 2.5 M *n*-BuLi solution in *n*-hexane (87 μL, 0.22 mmol) was added dropwise at -78 ℃, methylchlorosilane (28 μL, 0.22 mmol) was added after 0.5 h and the reaction was gradually warmed to 0 °C and stirred for 1 h. After silyl ether was detected by TLC, the reaction was cooled down to -78 ℃ again, *n*-BuLi (87 μL, 0.22 mmol) was added, after stirring for 15 min, 1-benzylpiperidine-4-carbaldehyde (0.33 mmol) was dropped into the reaction mixture. After the reaction was stirred for 2 h, quenched by saturated NH_4Cl, extracted with DCM (20 mL × 3), and the organic layers were washed with saturated $NaHCO_3$ and brine, dried over anhydrous Na_2SO_4. The solvent was evaporated under a vacuum, and the crude products were purified by column chromatography (DCM/CH_3OH, 30:1, v/v) to obtain intermediates **12a**(***Z***), **12a**(***E***), **12b** and **12c** with yields of 11% - 16%.

*(E)-2-((1-benzylpiperidin-4-yl)methylene)-5,6-dimethoxy-2,3-dihydrobenzo[b]thiophennnne 1,1-dioxide (**12a(E)**).*White solid, 11.1% yield. ^{1}H NMR (300 MHz, Chloroform-*d*) δ 7.30 (d, *J* = 15.9 Hz, 5H), 7.21 (s, 1H), 6.78 (s, 1H), 6.53 (d, *J* = 9.5 Hz, 1H), 3.93 (s, 6H), 3.82 (s, 2H), 3.53 (s, 2H), 2.93 (d, *J* = 9.8 Hz, 2H), 2.30 (s, 1H), 2.05 (t, *J* = 11.4 Hz, 2H), 1.67 (q, *J* = 13.0, 11.7 Hz, 4H). HR-MS (ESI) m/z: calcd for $C_{23}H_{28}NO_4S$ $[M+H]^+$ 414.1734, found 414.1740.

*(Z)-2-((1-benzylpiperidin-4-yl)methylene)-5,6-dimethoxy-2,3-dihydrobenzo[b]thiophene 1,1-dioxide (**12a(Z)**)*. White solid,11.1% yield. ^{1}H NMR (300 MHz, Chloroform-*d*) δ 7.37 (d, *J* = 15.9 Hz, 5H), 7.23 (s, 1H), 6.79 (s, 1H), 6.06 (d, *J* = 10.2 Hz, 1H), 4.05 – 3.95 (m, 7H), 3.89 (s, 2H), 3.61 (s, 2H), 3.40 – 3.17 (m, 1H), 3.00 (d, *J* = 10.1 Hz, 2H), 2.23 (t, *J* = 11.6 Hz, 2H), 1.96 (d, *J* = 12.9 Hz, 2H), 1.59 (d, *J* = 11.5 Hz, 2H). HR-MS (ESI) m/z: calcd for $C_{23}H_{28}NO_4S$ $[M+H]^+$ 414.1734, found 414.1742.

*(E)-2-((1-benzylpiperidin-4-yl)methylene)-6,7-dimethoxythiochromane 1,1-dioxide (**12b**)*. Yellow solid, 13.5% yield. ^{1}H NMR (300 MHz, Chloroform-*d*) δ 7.34 (s, 1H), 7.33 – 7.24 (m, 5H), 6.68 (s, 1H), 6.62 (d, *J* = 9.7 Hz, 1H), 3.90 (s, 3H), 3.88 (s, 3H), 3.50 (s, 2H), 3.03 (h, *J* = 5.7 Hz, 4H), 2.89 (d, *J* = 11.3 Hz, 2H), 2.32 (dq, *J* = 9.8, 4.7 Hz, 1H), 2.03 (td, *J* = 11.0, 4.1 Hz, 2H), 1.66 – 1.51 (m, 4H). ^{13}C NMR (75 MHz, Chloroform-*d*) δ 152.25, 148.29, 140.40, 138.01, 135.87, 131.10, 130.52, 129.20, 128.25, 127.10, 111.27, 105.94, 63.36, 56.26, 56.19, 52.81, 35.17, 31.11, 29.71, 28.42, 24.47. HR-MS (ESI) m/z: calcd for $C_{24}H_{30}NO_4S$ $[M+H]^+$ 428.1890, found 428.1895.

(E)-2-((1-benzylpiperidin-4-yl)methylene)-7,8-dimethoxy-2,3,4,5-tetrahydrobenzo[b]thiepine 1,1-dioxide (**12c**). Yellow solid, 16.2% yield. ^{1}H NMR (300 MHz, Chloroform-*d*) δ 7.49 (s, 1H), 7.31 (d, *J* = 4.1 Hz, 5H), 6.69 (s, 1H), 6.52 (d, *J* = 9.4 Hz, 1H), 3.93 (s, 3H), 3.91 (s, 3H), 3.52 (s, 2H), 3.21 (d, *J* = 9.7 Hz, 2H), 2.91 (t, *J* = 6.0 Hz, 4H), 2.27 (q, *J* = 8.3, 7.8 Hz, 1H), 2.02 (t, *J* = 6.1 Hz, 2H), 1.87 – 1.78 (m, 2H), 1.55 (dt, *J* = 9.5, 4.5 Hz, 4H). ^{13}C NMR (101 MHz, Chloroform-*d*) δ 152.07, 146.97, 143.10, 140.85, 134.75, 132.10, 129.29, 128.27, 127.22, 114.05, 109.97, 63.20, 56.30, 56.15, 52.72, 35.66, 34.69, 31.16, 29.72, 29.16, 28.14. HR-MS (ESI) m/z: calcd for $C_{25}H_{32}NO_4S$ $[M+H]^+$ 428.1890, found 428.1895.

*4.1.12. Synthesis of compound **12d***

3 mg Pd-C was added to a solution of compound **12a** (30 mg, 0.07 mmol) in MeOH (10 mL) and the reaction was stirred under H_2 for 2 h. The reaction solution was filtered and concentrated *in vacuo* to obtain the compound **12d** (27 mg, 0.06 mmol, 91% yield).

2-((1-benzylpiperidin-4-yl)methyl)-5,6-dimethoxy-2,3-dihydrobenzo[b]thiophene 1,1-dioxide (**12d**). Light yellow solid, 91.2 % yield ^{1}H NMR (300 MHz, Chloroform-*d*) δ 7.33 (d, J = 4.3 Hz,

5H), 7.15 (s, 1H), 6.72 (s, 1H), 3.92 (d, *J* = 2.2 Hz, 6H), 3.59 (d, *J* = 8.3 Hz, 1H), 3.54 (s, 2H), 3.30 (dd, *J* = 15.8, 7.7 Hz, 1H), 2.94 (d, *J* = 9.3 Hz, 2H), 2.91 – 2.83 (m, 1H), 2.12 – 1.99 (m, 3H), 1.89 – 1.72 (m, 2H), 1.70 – 1.60 (m, 2H), 1.39 (d, *J* = 10.1 Hz, 2H). ^{13}C NMR (75 MHz, Chloroform-*d*) δ 153.59, 149.84, 130.43, 129.72, 129.42, 128.28, 127.21, 108.11, 102.92, 63.27, 59.40, 56.34, 53.41, 34.54, 33.19, 32.47, 32.14, 31.94. HR-MS (ESI) m/z: calcd for $C_{23}H_{30}NO_4S$ $[M+H]^+$ 415.1817, found 415.1812.

*4.1.13. Synthesis of compound **16b***

The key intermediate **16b** shown in scheme 3 was successfully synthesized according to Liu's work [37].

*4.1.14. Synthesis of compounds **17a-b***

CH_3ONa (771 mg, 14.27 mmol) was added to a solution of compound **9a** (2.00 g, 9.51 mmol) in dry THF (20 mL) under an ice bath and the reaction, then compounds **16a-b** (11.42 mmol) was added. After the reaction was stirred at room temperature for 5 h, quenched with H_2O, extracted with DCM (50 mL × 3), the combined organic layers were washed with brine, dried over anhydrous Na_2SO_4. The solvent was evaporated under a vacuum, and the crude products were purified by column chromatography (DCM/CH_3OH, 50:1, v/v) to obtain compounds **17a-b** with yields of 62% - 68%.

*4.1.15. Synthesis of compounds **19a-b***

$NaBH_4$ (6.17 mmol) was added to a solution of compounds **17a-b** (1.23 mmol) in MeOH (20 mL) under an ice bath and the reaction was stirred for 0.5 h, quenched with saturated NH_4Cl. The MeOH was evaporated *in vacuo*, the residues were extracted with DCM (20 mL × 3), the combined organic layers were washed with brine, dried over anhydrous Na_2SO_4 and concentrated to obtain compounds **18a-b** with yields of 91% - 96%. Compounds **18a-b** (1.17 mmol) was dissolved in EtOH (20 mL), NH_4Cl solid (11.7 mmol) was added, and the reaction was refluxed for 3 h. The EtOH was removed under a vacuum, the resulting mixture was extracted with DCM (20 mL × 3), the combined organic layers were washed with brine, dried over anhydrous Na_2SO_4. The solvent was evaporated under a

vacuum, and the crude products were purified by column chromatography (DCM/CH_3OH, 100:1, v/v) to obtain compounds **19a-b** with yields of 72% - 80%.

*4.1.16. Synthesis of compounds **20a-b***

Similar to the reaction procedures for compounds **5a-5c**, *m*-CPBA (0.52 mmol) and $NaHCO_3$ solid (0.52 mmol) were added to a solution of **19a-b** (0.24 mmol) in dry DCM (20 mL), and the reaction was stirred at room temperature for 2 h. After a usual workup, the crude products were purified by column chromatography (DCM/CH_3OH, 30:1, v/v) to obtain compounds **20a-b** with yields of 72% - 80%.

*4.1.17. Synthesis of compounds **21a-b***

Similar to the reaction procedures for compound **12d**, 10 mg Pd-C was added to a solution of **20a-b** (0.19 mmol) in MeOH (10 mL) and the reaction was stirred under H_2 for 2 h. The reaction solution was filtered and concentrated *in vacuo* to obtain the compounds **21a-b** with yields of 89% - 95%.

*4.1.18. General Procedure for Synthesis of compounds **22a**, **23a** and **24a-q***

TFA (5 mL) was added to a solution of compound **19a**, **20a** or **21a-b** (0.38 mmol) in DCM (10 mL), and the reaction was stirred at room temperature for 2 h. The solvent was evaporated under a vacuum to obtain the corresponding products trifluoroacetic acid hydrochloride (yields: 70% - 75%), which were continuously dissolved in CH_3CN (10 mL), K_2CO_3 (3 eq) and corresponding substituted benzyl bromide (0.45 mmol) were added, and the reaction was stirred at room temperature for 0.5 h. The reaction mixture was extracted with DCM (20 mL × 3), the combined organic layers were washed with brine, dried over anhydrous Na_2SO_4. The solvent was evaporated under a vacuum, and the crude products were purified by column chromatography (DCM/CH_3OH, 30:1, v/v) to obtain compounds **22a**, **23a** and **24a-q** with yields of 45% - 66%.

*1-Benzyl-4-((5,6-dimethoxybenzo[b]thiophen-2-yl)methyl)piperidine (**22a**)*. Light yellow solid, 36.8% yield (two steps). ^{1}H NMR (300 MHz, Chloroform-*d*) δ 7.34 – 7.25 (m, 5H), 7.20 (s, 1H), 7.10 (s, 1H), 6.84 (s, 1H), 3.92 (s, 6H), 3.49 (s, 2H), 2.88 (d, J = 11.2 Hz, 2H), 2.77 (d, J = 6.9 Hz,

2H), 1.97 – 1.92 (m, 2H), 1.76 – 1.67 (m, 2H), 1.61 (ddq, *J* = 11.0, 7.4, 3.7 Hz, 1H), 1.35 (ddd, *J* = 11.6, 9.3, 3.5 Hz, 2H). ^{13}C NMR (101 MHz, Chloroform-*d*) δ 147.94, 147.48, 142.54, 138.29, 133.49, 131.79, 129.29, 128.17, 126.98, 121.20, 104.30, 103.97, 63.39, 56.16, 56.03, 53.67, 37.98, 37.77, 32.08. HR-MS (ESI) m/z: calcd for $C_{23}H_{28}NO_2S$ $[M+H]^+$ 382.1835, found 382.1843.

*2-((1-Benzylpiperidin-4-yl)methyl)-5,6-dimethoxybenzo[b]thiophene 1,1-dioxide (**23a**)*. Light yellow solid, 42.8% yield. ^{1}H NMR (400 MHz, Chloroform-*d*) δ 7.36 – 7.27 (m, 5H), 7.22 (s, 1H), 6.77 (s, 1H), 6.67 (s, 1H), 3.93 (s, 6H), 3.55 (s, 2H), 2.94 (d, *J* = 11.4 Hz, 2H), 2.50 (d, *J* = 7.1 Hz, 2H), 2.10 – 2.02 (m, 2H), 1.89 (dq, *J* = 7.5, 3.7 Hz, 1H), 1.81 (d, *J* = 13.1 Hz, 2H), 1.44 – 1.36 (m, 2H). ^{13}C NMR (101 MHz, Chloroform-*d*) δ 153.06, 150.10, 142.31, 129.43, 128.28, 127.26, 126.24, 124.91, 106.95, 104.67, 63.12, 56.49, 56.39, 53.28, 33.65, 31.87, 31.73. HR-MS (ESI) m/z: calcd for $C_{23}H_{28}NO_4S$ $[M+H]^+$ 414.1734, found 414.1739.

*2-((1-(4-Fluorobenzyl)piperidin-4-yl)methyl)-5,6-dimethoxy-2,3-dihydrobenzo[b]thiophene 1,1-dioxide (**24a**)*. Yellow solid, 45.3% yield. ^{1}H NMR (300 MHz, Chloroform-*d*) δ 7.28 (q, *J* = 5.3 Hz, 2H), 7.15 (s, 1H), 7.00 (t, *J* = 8.5 Hz, 2H), 6.72 (s, 1H), 3.92 (d, *J* = 2.7 Hz, 6H), 3.58 (t, *J* = 7.5 Hz, 1H), 3.47 (s, 2H), 3.31 (dd, *J* = 15.8, 7.7 Hz, 1H), 2.90 (dd, *J* = 10.0, 6.2 Hz, 3H), 2.02 (dt, *J* = 18.9, 8.6 Hz, 3H), 1.80 (dd, *J* = 27.2, 12.8 Hz, 2H), 1.65 (t, *J* = 8.4 Hz, 2H), 1.36 (dt, *J* = 12.1, 7.0 Hz, 2H). ^{13}C NMR (101 MHz, Chloroform-*d*) δ 161.99 (d, *J* = 244.8 Hz), 153.59, 149.83, 133.80, 130.73 (d, *J* = 7.9 Hz), 130.42, 129.69, 114.99 (d, *J* = 21.1 Hz), 108.11, 102.92, 62.48, 59.40, 56.32, 56.27, 53.37, 53.34, 34.54, 33.24, 32.46, 32.22, 32.04. HR-MS (ESI) m/z: calcd for $C_{23}H_{29}FNO_4S$ $[M+H]^+$ 434.1796, found 434.1809.

*2-((1-(3-Fluorobenzyl)piperidin-4-yl)methyl)-5,6-dimethoxy-2,3-dihydrobenzo[b]thiophene 1,1-dioxide (**24b**)*. White solid, 43.1% yield. ^{1}H NMR (300 MHz, Chloroform-*d*) δ 7.27 (q, *J* = 7.9, 7.2 Hz, 1H), 7.15 (s, 1H), 7.12 - 7.02 (m, 2H), 6.94 (t, *J* = 8.6 Hz, 1H), 6.72 (s, 1H), 3.92 (s, 3H), 3.92 (s, 3H), 3.58 (t, *J* = 7.5 Hz, 1H), 3.49 (s, 2H), 3.31 (dd, *J* = 15.8, 7.7 Hz, 1H), 2.89 (q, *J* = 6.9, 6.1 Hz, 3H), 2.05 (dq, *J* = 19.6, 10.1, 8.9 Hz, 3H), 1.80 (dd, *J* = 26.1, 12.8 Hz, 2H), 1.65 (t, *J* = 8.8 Hz, 2H), 1.37 (t, *J* = 13.0 Hz, 2H); ^{13}C NMR (75 MHz, Chloroform-*d*) δ 162.9 (d, *J* = 244.5 Hz), 153.59, 149.85, 141.22 (d, *J* = 6.8 Hz), 130.46, 129.66, 129.60 (d, *J* = 7.5 Hz), 124.54 (d, *J* = 3.0 Hz), 115.72 (d, J = 21.0 Hz), 113.82 (d, *J* = 21.0 Hz), 108.13, 102.96, 62.71, 59.44, 56.30, 56.25, 53.47, 34.56,

33.26, 32.48, 32.30, 32.14. HR-MS (ESI) m/z: calcd for $C_{23}H_{29}FNO_4S$ $[M+H]^+$ 434.1796, found 434.1809.

*2-((1-(2-Fluorobenzyl)piperidin-4-yl)methyl)-5,6-dimethoxy-2,3-dihydrobenzo[b]thiophene 1,1-dioxide (**24c**)*. White solid, 40.5% yield. ^{1}H NMR (300 MHz, Chloroform-*d*) δ 7.38 (t, *J* = 6.6 Hz, 1H), 7.27 – 7.19 (m, 1H), 7.16 – 6.99 (m, 3H), 6.72 (s, 1H), 3.92 (s, 3H), 3.92 (s, 3H), 3.60 (s, 2H), 3.57 (d, *J* = 11.6 Hz, 1H), 3.31 (dd, *J* = 15.8, 7.7 Hz, 1H), 2.94 (d, *J* = 9.6 Hz, 2H), 2.91 – 2.83 (m, 1H), 2.12 – 2.02 (m, 3H), 1.80 (dd, *J* = 25.3, 12.7 Hz, 2H), 1.70 – 1.55 (m, 2H), 1.43 – 1.32 (m, 2H). ^{13}C NMR (75 MHz, Chloroform-*d*) δ 161.52 (d, *J* = 235.5 Hz), 153.58, 159.83, 131.73 (d, *J* = 4.5 Hz), 130.43, 129.70, 128.79 (d, *J* = 8.3 Hz), 124.65 (d, *J* = 15.7 Hz), 123.85 (d, *J* = 3.4 Hz), 115.24 (d, *J* = 22.5 Hz), 108.10, 102.92, 69.24, 59.41, 56.32, 56.28, 55.50, 53.19, 34.50, 33.15, 32.43, 32.24, 32.16. HR-MS (ESI) m/z: calcd for $C_{23}H_{29}FNO_4S$ $[M+H]^+$ 434.1796, found 434.1805.

*2-((1-(2,4-Difluorobenzyl)piperidin-4-yl)methyl)-5,6-dimethoxy-2,3-dihydrobenzo[b]thiophene 1,1-dioxide (**24d**)*. Light yellow solid, 46.7% yield. ^{1}H NMR (300 MHz, Chloroform-*d*) δ 7.35 (q, *J* = 7.9 Hz, 1H), 7.15 (s, 1H), 6.90 – 6.75 (m, 2H), 6.72 (s, 1H), 3.93 (s, 3H), 3.92 (s, 3H), 3.60 (s, 1H), 3.55 (s, 2H), 3.31 (dd, *J* = 15.8, 7.7 Hz, 1H), 2.91 (d, *J* = 9.0 Hz, 2H), 2.87 (d, *J* = 11.5 Hz, 1H), 2.04 (d, *J* = 11.8 Hz, 3H), 1.81 (dd, *J* = 26.5, 12.8 Hz, 2H), 1.64 (t, *J* = 7.0 Hz, 2H), 1.42 – 1.32 (m, 2H). ^{13}C NMR (75 MHz, Chloroform-*d*) δ 153.59, 149.84, 132.49 (dd, *J* = 9.0 Hz, *J* = 6.0 Hz), 130.41, 129.68, 111.06 (dd, *J* = 20.5 Hz, *J* = 3.8 Hz), 108.10, 103.58 (t, *J* = 25.6 Hz), 102.91, 69.24, 59.38, 56.33, 56.28, 54.96, 53.12, 34.50, 33.10, 32.44, 32.18, 32.03. HR-MS (ESI) m/z: calcd for $C_{23}H_{28}F_2NO_4S$ $[M+H]^+$ 452.1702, found 452.1707.

*2-((1-(3-Chloro-4-fluorobenzyl)piperidin-4-yl)methyl)-5,6-dimethoxy-2,3-dihydrobenzo[b]thiophene 1,1-dioxide (**24e**)*. Yellow solid, 41.9% yield. ^{1}H NMR (300 MHz, Chloroform-*d*) δ 7.38 (dd, *J* = 7.1, 2.1 Hz, 1H), 7.15 (s, 2H), 7.07 (t, *J* = 8.6 Hz, 1H), 6.73 (s, 1H), 3.93 (s, 3H), 3.92 (s, 3H), 3.58 (t, *J* = 7.5 Hz, 1H), 3.44 (s, 2H), 3.31 (dd, *J* = 15.8, 7.7 Hz, 1H), 2.95 – 2.87 (m, 2H), 2.85 (s, 1H), 2.12 – 1.95 (m, 3H), 1.81 (dd, *J* = 27.9, 12.7 Hz, 2H), 1.71 – 1.58 (m, 2H), 1.35 (d, *J* = 11.2 Hz, 2H). ^{13}C NMR (75 MHz, Chloroform-*d*) δ 157.17 (d, *J* = 247.7 Hz), 153.59, 149.83, 135.53, 130.97, 130.40, 129.69, 128.67 (d, *J* = 7.1 Hz), 120.62 (d, *J* = 17.9 Hz),

116.22 (d, *J* = 20.7 Hz), 108.11, 102.90, 62.02, 59.38, 56.32, 56.28, 53.40, 34.55, 33.19, 32.47, 32.24, 32.02. HR-MS (ESI) m/z: calcd for $C_{23}H_{28}ClFNO_4S$ $[M+H]^+$ 468.1406, found 468.1413.

*5,6-Dimethoxy-2-((1-(2,4,6-trifluorobenzyl)piperidin-4-yl)methyl)-2,3-dihydrobenzo[b]thiophene 1,1-dioxide (**24f**).*White solid, 39.7% yield. ^{1}H NMR (300 MHz, Chloroform-*d*) δ 7.14 (s, 1H), 6.68 (dd, *J* = 15.0, 6.9 Hz, 3H), 3.92 (s, 3H), 3.91 (s, 3H), 3.65 (s, 2H), 3.57 (t, *J* = 7.6 Hz, 1H), 3.30 (dd, *J* = 15.8, 7.7 Hz, 1H), 2.93 (d, *J* = 10.4 Hz, 2H), 2.90 – 2.81 (m, 1H), 2.07 (dd, *J* = 12.5, 6.7 Hz, 3H), 1.80 (dd, *J* = 28.7, 12.9 Hz, 2H), 1.63 (q, *J* = 10.4, 8.9 Hz, 2H), 1.35 (td, *J* = 12.0, 3.7 Hz, 2H). ^{13}C NMR (75 MHz, Chloroform-*d*) δ 162.21 (d, *J* = 244.0 Hz), 153.57, 149.82, 130.42, 129.66, 108.08, 102.90, 100.01 (t, *J* = 27.6 Hz), 69.24, 59.35, 56.31, 56.27, 52.50, 48.64, 34.48, 32.91, 32.43, 32.24, 32.02. HR-MS (ESI) m/z: calcd for $C_{23}H_{27}F_3NO_4S$ $[M+H]^+$ 470.1607, found 470.1616.

*2-((1-Benzyl-4-fluoropiperidin-4-yl)methyl)-5,6-dimethoxy-2,3-dihydrobenzo[b]thiophene 1,1-dioxide (**24g**)*. White solid, 45.4% yield. ^{1}H NMR (400 MHz, Chloroform-*d*) δ 7.33 (d, *J* = 4.4 Hz, 4H), 7.26 (s, 1H), 7.16 (s, 1H), 6.73 (s, 1H), 3.92 (s, 3H), 3.92 (s, 3H), 3.66 (qd, *J* = 8.3, 3.9 Hz, 1H), 3.55 (s, 2H), 3.45 (ddd, *J* = 16.2, 7.9, 1.8 Hz, 1H), 3.03 (dd, *J* = 16.2, 8.4 Hz, 1H), 2.73 (t, *J* = 11.9 Hz, 2H), 2.37 (dd, *J* = 13.7, 5.3 Hz, 2H), 2.04 – 1.75 (m, 6H). ^{13}C NMR (101 MHz, Chloroform-*d*) δ 153.73, 149.88, 138.09, 130.06, 129.58, 129.11, 128.30, 127.18, 108.15, 102.95, 92.96 (d, *J* = 173.8 Hz), 62.85, 57.52, 56.32, 56.28, 48.92, 37.49 (d, *J* = 21.8 Hz), 36.36 (d, *J* = 21.0 Hz), 34.05 (d, J = 21.4 Hz), 33.30 (d, J = 3.3 Hz). HR-MS (ESI) m/z: calcd for $C_{23}H_{29}FNO_4S$ $[M+H]^+$ 434.1796, found 434.1803.

*2-((4-Fluoro-1-(4-fluorobenzyl)piperidin-4-yl)methyl)-5,6-dimethoxy-2,3-dihydrobenzo[b]thiophene 1,1-dioxide (**24h**)*. White solid, 47.2% yield. ^{1}H NMR (400 MHz, Chloroform-*d*) δ 7.33 – 7.27 (m, 2H), 7.16 (s, 1H), 7.02 (d, *J* = 8.7 Hz, 2H), 6.74 (s, 1H), 3.92 (s, 3H), 3.92 (s, 3H), 3.66 (qd, *J* = 8.4, 4.0 Hz, 1H), 3.51 (s, 2H), 3.45 (ddd, *J* = 16.1, 7.8, 1.7 Hz, 1H), 3.03 (dd, *J* = 16.1, 8.4 Hz, 1H), 2.72 (d, *J* = 11.7 Hz, 2H), 2.41 – 2.32 (m, 2H), 2.06 – 1.96 (m, 2H), 1.89 (d, *J* = 14.2 Hz, 2H), 1.87 – 1.70 (m, 2H). ^{13}C NMR (101 MHz, Chloroform-*d*) δ 162.06 (d, *J* = 245.0 Hz), 153.74, 149.89, 133.81, 130.56 (d, *J* = 7.9 Hz), 130.04, 129.56, 115.10 (d, *J* = 21.1 Hz), 108.15, 102.95, 92.90 (d, *J* = 173.8 Hz), 62.85, 57.52, 56.32, 56.28, 48.92, 37.52

(d, *J* = 22.2 Hz), 36.32 (d, *J* = 20.7 Hz), 34.03 (d, *J* = 21.2 Hz), 33.32 (d, *J* = 3.1 Hz). HR-MS (ESI) m/z: calcd for $C_{23}H_{28}F_2NO_4S$ $[M+H]^+$ 452.1702, found 452.1710.

*2-((4-Fluoro-1-(3-fluorobenzyl)piperidin-4-yl)methyl)-5,6-dimethoxy-2,3-dihydrobenzo[b]thiophene 1,1-dioxide (**24i**)*. White solid, 42.8% yield. ^{1}H NMR (400 MHz, Chloroform-*d*) δ 7.30 – 7.26 (m, 1H), 7.16 (s, 1H), 7.12 – 7.04 (m, 2H), 6.94 (td, *J* = 8.8, 8.3, 2.6 Hz, 1H), 6.74 (s, 1H), 3.92 (s, 3H), 3.92 (s, 3H), 3.67 (qd, *J* = 8.4, 3.9 Hz, 1H), 3.53 (s, 2H), 3.45 (ddd, *J* = 16.2, 7.8, 1.8 Hz, 1H), 3.03 (dd, *J* = 16.2, 8.4 Hz, 1H), 2.71 (t, *J* = 11.9 Hz, 2H), 2.43 – 2.34 (m, 2H), 2.06 – 1.96 (m, 2H), 1.89 (d, *J* = 10.7 Hz, 2H), 1.80 (d, *J* = 16.0 Hz, 2H). ^{13}C NMR (101 MHz, Chloroform-*d*) δ 162.96 (d, *J* = 245.3 Hz), 153.74, 149.89, 141.13 (d, *J* = 6.8 Hz), 130.05, 129.69 (d, *J* = 8.1 Hz), 124.45, 124.43, 115.63 (d, *J* = 21.1 Hz), 113.99 (d, *J* = 21.1 Hz), 108.16, 102.94, 92.88 (d, *J* = 173.7 Hz), 62.25, 57.50, 56.32, 56.28, 48.94,37.53 (d, *J* = 22.2 Hz), 36.38 (d, *J* = 20.8 Hz), 34.08 (d, *J* = 21.4 Hz), 33.32 (d, *J* = 3.2 Hz). HR-MS (ESI) m/z: calcd for $C_{23}H_{28}F_2NO_4S$ $[M+H]^+$ 452.1702, found 452.1710.

*2-((4-Fluoro-1-(2-fluorobenzyl)piperidin-4-yl)methyl)-5,6-dimethoxy-2,3-dihydrobenzo[b]thiophene 1,1-dioxide (**24j**)*. White solid, 43.4% yield. ^{1}H NMR (300 MHz, Chloroform-*d*) δ 7.38 (t, *J* = 7.4 Hz, 1H), 7.29 – 7.21 (m, 1H), 7.16 (s, 1H), 7.14 – 7.08 (m, 1H), 7.03 (t, *J* = 9.2 Hz, 1H), 6.73 (s, 1H), 4.00 – 3.84 (m, 6H), 3.66 (d, *J* = 5.2 Hz, 1H), 3.62 (s, 2H), 3.44 (dd, *J* = 16.1, 7.9 Hz, 1H), 3.02 (dd, *J* = 16.1, 8.3 Hz, 1H), 2.75 (s, 2H), 2.50 – 2.32 (m, 3H), 2.12 – 1.81 (m, 5H). ^{13}C NMR (101 MHz, Chloroform-*d*) δ 161.40 (d, *J* = 246.0 Hz), 153.71, 149.85, 131.50 (d, *J* = 4.4 Hz), 130.07, 129.53, 128.90 (d, *J* = 8.2 Hz), 124.66 (d, *J* = 14.8 Hz), 123.94 (d, *J* = 3.6 Hz), 115.30 (d, *J* = 22.2 Hz), 108.13, 102.90, 92.80 (d, *J* = 173.6 Hz), 57.50, 56.32, 56.29, 55.12, 48.72, 37.51 (d, *J* = 21.5 Hz), 36.35 (d, *J* = 20.8 Hz), 34.04 (d, *J* = 21.3 Hz), 33.29 (d, *J* = 3.3 Hz). HR-MS (ESI) m/z: calcd for $C_{23}H_{28}F_2NO_4S$ $[M+H]^+$ 452.1702, found 452.1704.

*2-((4-Fluoro-1-(2-fluorobenzyl)piperidin-4-yl)methyl)-5,6-dimethoxy-2,3-dihydrobenzo[b]thiophene 1,1-dioxide (**24k**)*.White solid, 36.7% yield. ^{1}H NMR (300 MHz, Chloroform-*d*) δ 7.47 (d, *J* = 7.3 Hz, 1H), 7.39 – 7.30 (m, 1H), 7.29 – 7.24 (m, 1H), 7.23 – 7.18 (m, 1H), 7.16 (s, 1H), 6.74 (s, 1H), 4.04 – 3.81 (m, 6H), 3.75 – 3.66 (m, 1H), 3.65 (s, 2H), 3.46

(dd, *J* = 15.7, 7.6 Hz, 1H), 3.04 (dd, *J* = 16.2, 8.4 Hz, 1H), 2.75 (t, *J* = 10.5 Hz, 2H), 2.47 (d, *J* = 11.2 Hz, 2H), 2.43 – 2.30 (m, 1H), 2.12 – 1.73 (m, 5H). ^{13}C NMR (101 MHz, Chloroform-*d*) *δ* 153.72, 149.86, 134.31, 130.63, 130.09, 129.54, 129.48, 128.24, 126.69, 108.13, 102.92, 92.87 (d, *J* = 173.8 Hz), 59.07, 57.52, 56.33, 56.30, 48.98, 37.52 (d, *J* = 21.4 Hz), 36.45 (d, *J* = 21.1 Hz), 34.08 (d, *J* = 21.3 Hz), 33.31 (d, *J* = 3.3 Hz). HR-MS (ESI) m/z: calcd for $C_{23}H_{28}F_2NO_4S$ $[M+H]^+$ 452.1702, found 452.1704.

*2-((1-(3-Chlorobenzyl)-4-fluoropiperidin-4-yl)methyl)-5,6-dimethoxy-2,3-dihydrobenzo[b]thiophene 1,1-dioxide (**24l**)*. Light yellow solid, 38.8% yield. ^{1}H NMR (300 MHz, Chloroform-*d*) *δ* 7.34 (s, 1H), 7.24 (q, *J* = 5.5, 5.0 Hz, 3H), 7.16 (s, 1H), 6.74 (s, 1H), 3.92 (s, 6H), 3.67 (dd, *J* = 8.4, 3.6 Hz, 1H), 3.51 (s, 2H), 3.48 – 3.36 (m, 1H), 3.03 (dd, *J* = 16.1, 8.3 Hz, 1H), 2.70 (t, *J* = 10.4 Hz, 2H), 2.52 – 2.31 (m, 3H), 2.15 – 1.80 (m, 5H). ^{13}C NMR (101 MHz, Chloroform-*d*) *δ* 153.71, 149.86, 140.52, 134.21, 130.05, 129.57, 129.54, 128.95, 127.32, 127.09, 108.13, 102.91, 92.87 (d, *J* = 173.7 Hz), 62.22, 57.49, 56.33, 56.29, 48.93, 37.52 (d, *J* = 21.8 Hz), 36.36 (d, *J* = 20.8 Hz), 34.05 (d, *J* = 21.3 Hz), 33.32 (d, *J* = 3.2 Hz). HR-MS (ESI) m/z: calcd for $C_{23}H_{28}FClNO_4S$ $[M+H]^+$ 468.1406, found 468.1409.

*2-((4-Fluoro-1-(2-methylbenzyl)piperidin-4-yl)methyl)-5,6-dimethoxy-2,3-dihydrobenzo[b]thiophene 1,1-dioxide (**24m**)*, White solid, 48.7% yield. ^{1}H NMR (300 MHz, Chloroform-*d*) *δ* 7.27 (d, *J* = 4.8 Hz, 1H), 7.16 (s, 4H), 6.73 (s, 1H), 3.92 (s, 6H), 3.71 – 3.60 (m, 1H), 3.50 (s, 2H), 3.47 – 3.37 (m, 1H), 3.03 (dd, *J* = 16.1, 8.3 Hz, 1H), 2.69 (d, *J* = 11.1 Hz, 2H), 2.50 – 2.32 (m, 6H), 2.14 – 1.79 (m, 5H). ^{13}C NMR (101 MHz, Chloroform-*d*) *δ* 153.74, 149.89, 137.55, 130.36, 130.33, 130.13, 129.82, 129.58, 127.16, 125.61, 108.18, 102.94, 93.09 (d, J = 175.5 Hz), 60.59, 57.55, 56.36, 56.33, 49.02, 37.48 (d, *J* = 20.2 Hz), 36.48 (d, *J* = 21.9 Hz), 34.15 (d, *J* = 19.6 Hz), 33.31, 19.31. HR-MS (ESI) m/z: calcd for $C_{24}H_{31}FNO_4S$ $[M+H]^+$ 448.1952, found 448.1956.

*2-((4-Fluoro-1-(2-(trifluoromethyl)benzyl)piperidin-4-yl)methyl)-5,6-dimethoxy-2,3-dihydrobenzo[b]thiophene 1,1-dioxide (**24n**)*. White solid, 47.4% yield. ^{1}H NMR (300 MHz, Chloroform-*d*) *δ* 7.79 (d, *J* = 7.8 Hz, 1H), 7.63 (d, *J* = 7.8 Hz, 1H), 7.52 (t, *J* = 7.5 Hz, 1H), 7.33 (t, *J* = 7.5 Hz, 1H), 7.16 (s, 1H), 6.74 (s, 1H), 3.99 – 3.86 (m, 6H), 3.70 (s, 2H), 3.68 – 3.55 (m, 1H),

3.46 (dd, *J* = 16.0, 7.9 Hz, 1H), 3.04 (dd, *J* = 16.2, 8.4 Hz, 1H), 2.70 (t, *J* = 10.2 Hz, 2H), 2.52 – 2.33 (m, 3H), 2.15 – 1.80 (m, 5H). ^{13}C NMR (101 MHz, Chloroform-*d*) δ 153.73, 149.86, 137.93, 131.80, 130.13, 129.51, 128.69, 128.39, 126.81, 125.74 (q, *J* = 6.0 Hz), 123.11, 108.15, 102.90, 92.86 (d, *J* = 173.7 Hz), 58.05, 57.54, 56.32, 56.29, 49.06 (d, *J* = 6.3 Hz), 37.56 (d, *J* = 21.8 Hz), 36.62 (d, *J* = 20.9 Hz), 34.13 (d, *J* = 21.3 Hz), 33.31 (d, *J* = 3.3 Hz). HR-MS (ESI) m/z: calcd for $C_{24}H_{28}F_4NO_4S$ $[M+H]^+$ 502.1670, found 502.1674.

*2-((1-(2,4-difluorobenzyl)-4-fluoropiperidin-4-yl)methyl)-5,6-dimethoxy-2,3-dihydrobenzo[b]thiophene 1,1-dioxide (**24o**)*. Light yellow solid, 40.5% yield. ^{1}H NMR (300 MHz, Chloroform-*d*) δ 7.36 (q, *J* = 8.3 Hz, 1H), 7.16 (s, 1H), 6.95 – 6.68 (m, 3H), 3.92 (s, 6H), 3.65 (dt, *J* = 8.5, 4.1 Hz, 1H), 3.57 (s, 2H), 3.45 (dd, *J* = 15.9, 7.9 Hz, 1H), 3.02 (dd, *J* = 16.1, 8.4 Hz, 1H), 2.71 (d, *J* = 9.9 Hz, 2H), 2.51 – 2.28 (m, 3H), 2.13 – 1.72 (m, 5H). ^{13}C NMR (101 MHz, Chloroform-*d*) δ 163.03 (dd, *J* = 87.9, 12.1 Hz), 160.51 (dd, *J* = 88.4, 12.0 Hz), 153.72, 149.86, 132.24 (dd, *J* = 9.5, 6.1 Hz), 130.04, 129.50, 120.54 (d, *J* = 16.4 Hz), 111.11 (dd, *J* = 20.9, 3.8 Hz), 108.12, 103.65 (t, *J* = 25.7 Hz), 102.89, 92.72 (d, *J* = 173.6 Hz), 57.47, 56.32, 56.29, 54.61, 48.62, 37.51 (d, *J* = 21.6 Hz), 36.27 (d, *J* = 21.1 Hz), 33.98 (d, *J* = 21.4 Hz), 33.29 (d, *J* = 3.3 Hz). HR-MS (ESI) m/z: calcd for $C_{23}H_{27}F_3NO_4S$ $[M+H]^+$ 470.1607, found 470.1610.

*2-((1-(3-Chloro-4-fluorobenzyl)-4-fluoropiperidin-4-yl)methyl)-5,6-dimethoxy-2,3-dihydrobenzo[b]thiophene 1,1-dioxide (**24p**)*. Light yellow solid, 45.7% yield. ^{1}H NMR (300 MHz, Chloroform-*d*) δ 7.43 – 7.33 (m, 1H), 7.17 (d, *J* = 6.6 Hz, 2H), 7.08 (t, *J* = 8.6 Hz, 1H), 6.74 (s, 1H), 3.93 (s, 6H), 3.66 (dt, *J* = 8.2, 4.0 Hz, 1H), 3.47 (s, 2H), 3.42 (d, *J* = 7.9 Hz, 1H), 3.03 (dd, *J* = 16.0, 8.3 Hz, 1H), 2.68 (t, *J* = 10.6 Hz, 2H), 2.42 (ddd, *J* = 31.3, 12.6, 3.7 Hz, 3H), 2.13 – 1.79 (m, 5H). ^{13}C NMR (101 MHz, Chloroform-*d*) δ 157.22 (d, *J* = 247.9 Hz), 153.73, 149.87, 135.50 (d, *J* = 2.0 Hz), 130.84, 130.03, 129.52, 128.49 (d, *J* = 7.1 Hz), 120.74 (d, *J* = 17.8 Hz), 116.30 (d, *J* = 20.9 Hz), 108.12, 102.90, 92.83 (d, *J* = 173.7 Hz), 61.57, 57.47, 56.33, 56.29, 48.86, 37.53 (d, *J* = 21.8 Hz), 36.34 (d, *J* = 20.8 Hz), 34.03 (d, *J* = 21.3 Hz), 33.32 (d, *J* = 3.1 Hz). HR-MS (ESI) m/z: calcd for $C_{23}H_{27}F_2ClNO_4S$ $[M+H]^+$ 486.1312, found 486.1319.

*2-((4-Fluoro-1-(3-methylbenzyl)piperidin-4-yl)methyl)-5,6-dimethoxy-2,3-dihydrobenzo[b]thiophene 1,1-dioxide (**24q**)*. White solid, 42.2% yield. ^{1}H NMR (300 MHz,

Chloroform-*d*) δ 7.27 – 7.05 (m, 5H), 6.73 (s, 1H), 3.92 (s, 6H), 3.66 (dd, *J* = 8.5, 3.4 Hz, 1H), 3.50 (s, 2H), 3.48 – 3.36 (m, 1H), 3.02 (dd, *J* = 16.1, 8.3 Hz, 1H), 2.72 (t, *J* = 9.7 Hz, 2H), 2.50 – 2.30 (m, 6H), 2.11 – 1.77 (m, 5H). ^{13}C NMR (101 MHz, Chloroform-*d*) δ 153.70, 149.85, 138.11, 137.91, 130.10, 129.85, 129.54, 128.16, 127.90, 126.22, 108.15, 102.89, 93.01 (d, *J* = 173.5 Hz), 62.93, 57.53, 56.32, 56.29, 48.97, 37.49 (d, *J* = 21.7 Hz), 36.39 (d, *J* = 20.9 Hz), 34.05 (d, *J* = 21.2 Hz), 33.30 (d, *J* = 3.2 Hz), 21.43. HR-MS (ESI) m/z: calcd for $C_{24}H_{31}FNO_4S$ $[M+H]^+$ 448.1952, found 448.1948.

*4.1.19. Synthesis of compound **26a***

Similar to the reaction procedures for compound **12d**, 100 mg Pd-C was added to a solution of compound **17a** (1.16 g, 2.86 mmol) in MeOH (50 mL) and the reaction was stirred under H_2 for 2 h. The reaction solution was filtered and concentrated *in vacuo* to obtain compound **25a** (1.00 g, 2.45 mmol, 86% yield). Then similar to the reaction procedures for compounds **5a-c**, compound **25a** was dissolved in DCM (20 mL) directly, $NaHCO_3$ (823 mg, 9.80 mmol) and *m*-CPBA (931 mg, 5.39 mmol) was added and the reaction was stirred at room temperature for 2 h. After a usual workup, the crude products (compound **26a**, 842 mg, 78% yield) were directly used for the next step.

*4.1.20. Synthesis of compound **27a***

K_2CO_3 (665 mg, 4.81 mmol) was added to a solution of compound **26a** (1.41 g, 3.21 mmol) in CH_3CN (20 mL), NFSI (1.7 g, 5.39 mmol) was added. After the reaction was stirred at room temperature for 1 h, then extracted with DCM (50 mL × 3), the combined organic layers were washed with saturated brine, dried over anhydrous Na_2SO_4, the solvent was evaporated under a vacuum to obtain compound **27a** (818 mg, 1.79 mmol, 56% yield), which was used for the next step directly.

*4.1.21. Synthesis of compound **28a***

Similar to the reaction procedures for **22a, 23a** and **24a-q**, TFA (10 mL) was added to a solution of compound **27a** (714 mg, 1.56 mmol) in DCM (20 mL), and the reaction was stirred at room temperature for 2 h. The solvent was evaporated under a vacuum to obtain the corresponding product

trifluoroacetic acid hydrochloride (560 mg, 1.19 mmol, 76% yield), which was continuously dissolved in CH_3CN (20 mL), K_2CO_3 (542 mg, 3.92 mmol) and 3-flurinebenzyl bromide (337 mg, 1.78 mmol) were added, and the reaction was stirred at room temperature for 0.5 h. After a usual workup, the crude product (compound **28a**, 233 mg, 42% yield) was used in the next step directly.

*4.1.22. Synthesis of compound **24r***

The synthesis procedure of compound **29a** was similar to the reaction procedures for compounds **18a-b**, $NaBH_4$ (61 mg, 1.61 mmol) was added to a solution of compound **28a** (500 mg, 1.07 mmol) in MeOH (20 mL) under an ice bath and the reaction was stirred for 0.5 h. After a usual workup, the crude product compound **29a** (420 mg, 0.90 mmol, 84% yield) was dissolved in DCM directly and the solution was degasified with N_2. pyridine (426 mg, 5.39 mmol) and Phenyl chlorothionocarbonate (620 mg, 3.59 mmol) were added dropwise under an ice bath, the reaction was warmed to room temperature and stirred for 3h. The reaction mixture was extracted with DCM (20 mL × 3), the combined organic layers were washed with saturated brine, dried over anhydrous Na_2SO_4, and the solvent was evaporated under a vacuum, and the crude products were purified by column chromatography (DCM/CH_3OH, 100:1, v/v) to obtain compound **30a** (290 mg, 0.48 mmol, 53% yield). Compound **30a** (290 mg, 0.48 mmol) was dissolved in toluene (20 mL) and the solution was degasified with N_2. Catalytic amount of AIBN and tri-n-butyltin hydride (419 mg, 1.44 mmol) were added, the reaction was refluxed for 2 h, the solvent was evaporated under a vacuum, and the crude products were purified by column chromatography (DCM/CH_3OH, 30:1, v/v) to obtain compound **24r** (139 mg, 0.31mmol, 64% yield).

*2-Fluoro-2-((1-(3-fluorobenzyl)piperidin-4-yl)methyl)-5,6-dimethoxy-2,3-dihydrobenzo[b]thiophene 1,1-dioxide (**24r**)*. White solid, 63.9% yield. ^{1}H NMR (300 MHz, Chloroform-*d*) δ 7.26 (td, *J* = 7.9, 6.7, 4.5 Hz, 1H), 7.16 (s, 1H), 7.07 (t, *J* = 7.4 Hz, 2H), 6.93 (td, *J* = 8.6, 2.6 Hz, 1H), 6.74 (s, 1H), 3.91 (s, 6H), 3.48 (s, 2H), 3.40 (s, 1H), 3.31 (d, *J* = 5.6 Hz, 1H), 2.86 (d, *J* = 11.2 Hz, 2H), 2.25 (ddd, *J* = 34.0, 13.6, 5.6 Hz, 2H), 2.06 (td, *J* = 12.8, 12.1, 7.4 Hz, 3H), 1.87 (t, *J* = 8.3 Hz, 2H), 1.52 – 1.39 (m, 2H). ^{13}C NMR (75 MHz, Chloroform-*d*) δ 162.38 (d, *J* = 245.2 Hz), 153.67, 149.59, 140.68 (d, *J* = 7.0 Hz), 129.06 (d, *J* = 8.1 Hz), 126.79 (d, *J* = 15.3 Hz), 124.04 (d, *J* = 2.8 Hz), 115.19 (d, *J* = 21.2 Hz), 113.30 (d, *J* = 21.2 Hz), 110.25, 108.24, 107.27,

103.33, 62.15, 62.12, 55.83, 55.79, 52.94, 52.91, 37.13 (d, *J* = 23.9 Hz), 36.60 (d, *J* = 20.6 Hz), 32.58 (d, *J* = 14.5 Hz), 31.00. HR-MS (ESI) m/z: calcd for $C_{23}H_{28}F_2NO_4S$ $[M+H]^+$ 452.1702, found 452.1663.

*4.1.23. Synthesis of **24r-HCl***

12 mL of HCl in EtOH (1.0 M) was slowly added to a solution of **24r** (500 mg, 1.14 mmol) in EtOH (5 mL). Then, the solvent was removed by filtration to obtain **24r-HCl** (498 mg, 1.05 mmol, 92% yield).

4.2. Pharmacology

4.2.1. AChE inhibitory activity assay in vitro

The Ellman's method was used to test the inhibitory activity against AChE of all compounds [32]. The cortex of mice was homogenized in a 30-fold volume of sodium phosphate buffer (0.075 M, pH 7.4, 0 ℃) containing tetraisopropylpyrophosphoramide (iso-OMPA, 0.4 mM) in a glass homogenizer, then the homogenate was centrifuged at 5000 g for 10 minutes to get the AChE source. The test compounds were dissolved in DMSO (1%, v/v) and diluted to the desired concentration with Tris-HCl buffer solution (50 mM Tris-HCl, pH = 8.0, 0.1 M NaCl, 0.02 M $MgCl_2 \cdot 6H_2O$, 25 ℃). Then 160 μL 1.5 mM 5,5'-dithiobis (2-nitrobenzoic acid) (DTNB, Ellman's reagent), 50 μL AChE (0.22 U/mL prepared in 50 mM Tris-HCl) and 10 mL of various concentrations of test compounds were added into the 96-well plates sequentially. After incubation at room temperature for 10 min, 30 μL acetylthiocholine iodide (15 mM) as the substrate of the AChE was added quickly. The absorbance was measured at different time intervals (0, 60, 120 and 180 s) at 405 nm. Then the inhibition rate was measured and the IC_{50} value was calculated (the IC_{50} value was defined as the concentration of the compound that reduced 50% of the enzymatic activity without inhibitor. Results are expressed as the mean ± SEM of three different experiments performed in triplicate.

4.2.2. Molecular modeling

In current research, the complex of recombinant human AChE and donepezil was downloaded from the Protein Data Bank (PDB code: 4EY7). The structure was edited by the Protein and Ligand

Preparation module accordingly in Schrodinger and it was minimized using the OPLS-2005 force field. The Glide program was used to study the possible mode of interaction, and the size of bounding box was defined as 10 Å × 10 Å × 10 Å. Then the preprocessing of the protein was conducted with Protein Preparation Wizard, and compound **24r** and other representative compounds (**12a**(***E***), **12a**(***Z***) and **24b**) are prepared with LigPrep, both in Schrodinger software, and were minimized using the OPLS-2005 force field. The molecular docking between compounds and enzymes was performed using the Glide standard precision (Glide-SP) mode with the ligands as flexible, the force field was set as OPLS-2005, and all other parameters were set to default. We also performed a re-docking experiment for validation of the used docking protocol and found that RMSD = 0.1603, indicating the docking experiment is reliable. Subsequently, PyMOL software was used to process docking results as figures.

4.2.3. Kinetic study of AChE inhibition

The kinetic study of AChE was carried out with two different concentrations (1.25 and 2.5 nM) of compound **24r** by Ellman's method. Lineweaver-Burk reciprocal plots (1/v *vs.* 1/[s]) were constructed at varying concentrations of the substrate acetylthiocholine (0.1 - 0.4 mM) to obtain the type of inhibition. Lineweaver-Burk secondary plots were constructed at obtained slope. Data analysis was performed with Graph Pad Prism 4.03 software (San Diego, CA, USA).

4.2.4. SH-SY5Y culture and neuronal differentiation

SH-SY5Y cells were cultured on different media detailed in Table 6 and differentiated as described previously by Shipley with some modifications [50]. Briefly, cells were seeded with basic growth media and allowed to reach 70% confluency. Subsequently, media was changed to differentiation media #1 and replaced every other day for the following 7 days. Cells were then passaged 1:1 and moved into fresh plates and differentiation media #2 was added. Media #2 was then replaced every 48 hours for 4 days. Lastly, media was changed with differentiation media #3 and replaced every 48 hours for the following week. Following this period, SH-SY5Y differentiated neuronal cells were used for the subsequent assays and analysis.

Table 6. Cell culture media for SH-SY5Y neuronal differentiation.

Basic Growth Media	Differentiation Media #1	Differentiation Media #2	Differentiation Media #3
EMEM	EMEM	EMEM	Neurobasal
15% hiFBS	2.5% hiFBS	1% FBS	20 mM KCl
1x Pen/Strep	1x Pen/Strep	1x Pen/Strep	1x Pen/Strep
2 mM Glutamine	2 mM Glutamine	2 mM Glutamine	2 mM Glutamax
	10 μM RA	10 μM RA	10 μM RA
			50 ng/ml BDNF

4.2.5. Glyceraldehyde (GA) induced tau hyperphosphorylation

In order to induce tau hyperphosphorylation, differentiated SH-SY5Y neuronal cells were treated with 1 mM GA for 24 hours as previously described [51]. Following incubation with GA, SH-SY5Y differentiated neuronal cells were used in the downstream assays.

4.2.6. Intracellular assay of AChE inhibitory activity

AChE activity was assessed using an AChE assay kit (#ab138871, Abcam plc.) following the manufacturer's instruction of Ellman's method. A total of 10^5 per well were seeded into a clear 96-well plate. After appropriate differentiation and drug treatment, cell culture media was removed, and 100 μL of lysis buffer were added into each well and left to incubate for 15 minutes at room temperature. Subsequently, 50 μL of acetylthiocholine reaction mixture (1X assay buffer, 1X DTNB stock solution, 1X acetylthiocholine stock solution) were added to each well and samples were left to incubate for 30 minutes at room temperature. Samples were then analyzed using a 96-well microplate reader at OD = 410 nm. In order to avoid false positive given by butyrylcholinesterase activity, the specific AChE inhibitor donepezil hydrochloride was used as control.

4.2.7. Cell viability assay

A total of 105 per well were seeded into a 96-well plate. After SH-SY5Y differentiation, cells were treated with 1 mM GA. Along with GA treatment, an appropriate concentration of the compound to be tested was added. After 24 hours, 25 μL of 5 mg/ml Methylthiazolyldiphenyl-tetrazolium bromide (MTT) (#M2128-100MG, Sigma-Aldrich) were added into each well without

removing cell culture media and incubated at 37 °C with 5% CO_2 for 2 hours. Subsequently, 100 µL of lysing buffer (50% SDS solution, 25% DMF, 25% demineralised water) were added. After an overnight incubation (20 h) at 37 °C, the optical densities at 490 nm were measured using 96-well plate reader. The medium/MTT/lysing buffer incubated under the same conditions was used as the control.

4.2.8. Quantification of p-Tau and total tau levels

Phosphorylation levels of tau protein at S199 and S396 were quantified using Enzyme Linked Immunosorbent Assay methodology. Following the manufacturer recommended protocol, ELISA kits KHB7041, KHB7031, and KHB0041 (ThermoFisher Scientific) were used to quantify phosphorylated tau S199, phosphorylated S396, and total tau respectively. Phosphorylation percentage was obtained, for the analyzed residues, by normalization against total tau.

4.2.9. Immunostaining cell culture

SH-SY5Y cells and differentiated SH-SY5Y cells were fixed in 4% PFA for 10 minutes at minutes at room temperature. Each sample was then washed three times with 0.1% PBS-T for 2 minutes. Following fixation, cells were incubated at room temperature for 2 hours in 5% NGS-T blocking solution, and incubated overnight at 4 °C with the mouse monoclonal anti-tubulin III primary antibody (#ab179513, Abcam plc.) at a final concentration of 1:1000. Primary antibody was then removed, and each sample was washed three times with 0.1% PBS-T. Rabbit anti-mouse secondary antibody Alexa Fluor 488 (#ab150113, Abcam plc.) was then added at a final 1:2000 concentration, and left to incubate at RT for 1 hour. Secondary antibody was then removed, and each sample was washed three times with 0.1% PBS-T. Samples were then mounted on to glass slide, using FluoroGel Mounting media (Genetex). Samples were then imaged by confocal microscopy within 24 hours.

4.2.10. Morphological analysis

Morphological analysis of SH-SY5Y differentiated neuronal cells confocal images was performed using ImageJ plug-in NeuronJ. Three more random areas were analyzed. A threshold

mask was applied to visualize the axon only and not the cell body. Subsequently, measurement of the axon length was taken, and distance between coordinates was measured with NeuronJ.

4.2.11. Quantification of AChE-induced Aβ42 aggregation

Measurements of AChE-induced amyloid aggregation were taken. Briefly, hexafluoroisopropanol (HFIP)-treated E22G Aβ peptides (#SP-Ab-11_0.1, JPT - Innovative Peptide Solution) were dissolved in DMSO to reach a final 200 µM stock. The dissolved peptides were subsequently centrifuged at 13500 g for 10 minutes, the supernatant was then transferred into a fresh vial used for the following experiments. To evaluate the aggregation rate in presence of AChE inhibitors, 2 µL of the compound of interest (at the appropriate concentration) were added into each vial, followed by 2 µL of 200 µM Aβ peptides stock, 20 µL AChE enzyme (#C3389-500UN, Sigma-Aldrich ltd) (2 U/mL, in 1X PBS at pH 8.0), and 76 µL of 1X PBS pH 8.0. The reaction was then incubated at RT for 24 hours. Subsequently, 100 µL of 5 µM Thioflavin T (ThT) were added into each vial. After one-hour incubation at RT, fluorescence emission was recorded at 490 nm with an excitation wavelength of 450 nm using a Tecan Spark microplate reader. Results were then processed as done using the subsequent formula: (Fi - Fb) / (Fo - Fb) x 100. Where Fi correspond to amyloid aggregation in presence of peptides, AChE, AChE inhibitors and ThT; Fo represents the amyloid aggregation in presence of peptides, AChE and ThT; Fb corresponds to blank control containing ThT only.

4.2.12. JC-1 assay for mitochondrial health

Changes in mitochondrial membrane potential (MMP) as a measure of mitochondrial dysfunction in response to okadaic acid, were assessed using dual emission potential-sensitive JC-1 probe (5,5',6,6'-tetrachloro-1,1',3,3'-tetraethyl-benzimidazolyl-carbocyanine iodide). JC-1 is a fluorescent lipophilic dye that selectively accumulates in mitochondria and changes from red fluorescence in cells with healthy MMP to green fluorescence with mitochondrial membrane depolarization that signifies mitochondrial dysfunction. SH-SY5Y cells were seeded at a density of 20,000 cells per well in a 96-well clear bottom plate and cultured for 24 h at 37 °C with 5% CO_2. After 24 h the cells were exposed to vehicle, donepezil or **24r** for 24 h, then treated for a further 24

h with 0.03 μM okadaic acid. Following treatment, cells were washed once with PBS and then incubated with 2 μM JC-1 dye for 30 mins at 37 °C with 5% CO_2. The dye was removed, and cells were washed three times with PBS, 100 μL of fresh PBS was added to each well. Green fluorescence was measured using a microplate reader at wavelengths of 485 nm excitation and 535 nm emission, while red fluorescence was measured at 535 nm excitation and 595 nm emission.

4.2.13. DCF assay for ROS level measurement

Intracellular ROS levels were determined using 2',7'-Dichlorofluorescin diacetate (DCFH-DA). When applied to intact cells, DCFH-DA crosses the cell membranes and is converted by intracellular esterase to non-fluorescent DCFH. However, in the presence of ROS, DCFH is oxidised to fluorescent 2',7'-Dichlorofluorescein (DCF), which can be used to quantify intracellular ROS in the cells. SH-SY5Y cells were seeded at a density of 20,000 cells per well in a 96-well clear bottom plate and cultured for 24 h at 37 °C with 5% CO_2. After 24 h the cells were exposed to vehicle, donepezil or **24r** for 24 h, then treated for a further 24 h with 0.03 μM okadaic acid. Following treatment, cells were incubated with 40 μM DCFH-DA for 30 mins at 37 °C with 5% CO_2. The dye was removed, and cells were washed three times with PBS, 100 μL of fresh PBS was added to each well and fluorescence was measured using a microplate reader at wavelengths of 485 nm excitation and 535 nm emission.

4.2.14. Cytochrome P450 inhibition assay

Cytochrome P450 inhibition was assessed in human liver microsomes (HLMs, 0.25 mg/mL) using four specific probe substrates (CYP2C9, 5 μM diclofenac; CYP2D6, 5 μM dextromethorphan; CYP3A4-M, 2.5 μM midazolam and CYP3A4-T, 50 μM testosterone) in the presence of multiple concentrations of the test compound (0.05-20 μM). After pre-incubation for 10 min at 37 ℃, the reaction was initiated by adding 20 μL NADPH to a final concentration of 10 mM. The mixture was incubated at 37 ℃ for 10 min and the reaction was terminated by adding 400 μL cold stop solution (200 ng/mL tolbutamide and 200 ng/mL labetalol in acetonitrile). After the reactions were terminated, the plates were centrifuged, and the supernatants were analyzed by LC/MS/MS.

4.2.15. BBB permeability assay

LC-MS/MS system was employed in this assay to detect the concentration of compound **24r** in the plasma and brain. We first established the two standard curves with LC-MS/MS by setting the concentration of compound **24r** in plasma and brain tissues to 0.50, 1.00, 2.00, 5.00, 10.0, 40.0, 200, 500, 900, 1000 ng/mL, respectively. The experimental protocols were evaluated and approved by the Ethics Committee of the China Pharmaceutical University (IACUC NO. 2020-06-004). A total of 15 adult female ICR mice were divided into five groups (n = 3) randomly, and treated with **24r-HCl** at a dosage of 1 mg/kg (i.g.). Blood and brain tissues were collected after 0.25 h, 0.5 h, 1 h, 2 h, 4 h for administration. The collected blood samples were placed in an EDTA-K2 anticoagulant tube on an ice bath, centrifuged at 4 ℃ and 8000 rpm for 5 minutes, and the obtained plasma was transferred to -20 ℃ for storage at once. The brain tissues were peeled off the surface blood vessels with filter paper, and were put into the corresponding numbered seal bag and stored at -20 ℃ for testing. According to the established standard curve, the concentration of compound **24r** in the brain and plasma were detected respectively at each time point, and the ratio of brain/plasma was calculated.

4.2.16. In vivo inhibitory activities assay

The experimental protocols were evaluated and approved by the Ethics Committee of the China Pharmaceutical University (IACUC NO. 2020-06-004). All the mice were treated with **24r-HCl** (0.5, 1, 2, 4 mg/kg) or donepezil (10 mg/kg, as a positive control) by intragastric administration (i.g.) respectively (the control group was treated with distilled water). The mice were sacrificed at 1 h after drug administration, the brain was taken out and the cortex and hippocampus of mice were dissected on ice quickly. Then the cortex and hippocampus were homogenized in a 30-fold volume of phosphate buffer (0 ℃, 0.075 M, pH 7.4) with iso-OMPA (0.4 mM). Next, 20 μL of obtained homogenate of cortex or hippocampus were incubated with a 250 μL of reaction mixture (100 μL of ddH_2O, 50 μL of phosphate buffer (0.1 M, pH 7.4), 30 μL of acetylthiocholine iodide (2 mM), 50 μL of DTNB (0.2%)) at room temperature. After 20 min, 50 μL of 3% sodium dodecyl sulfate (SDS) was added to terminate the reaction. Finally, the absorbance was measured by a microplate reader at 450 nm and the protein concentration was determined with BCA method. The obtained data were normalized by the AChE activity of vehicle-treated group.

4.2.17. Behavioral studies

The step-through passive avoidance test was carried out in shuttle box to evaluate learning and memory function of scopolamine-induced cognition-impaired mice. The shuttle box consists of two compartments of the same size, bright compartment and dark compartment (20.3 cm × 15.9 cm × 21.3 cm), The two compartments are connected by an arched door (8.9 cm × 11.4 cm), mice could shuttle freely. The floor on dark compartment was connected to the stimulator and could give electric foot shock, and the bright compartment is not. The experimental protocols were evaluated and approved by the Ethics Committee of the China Pharmaceutical University (IACUC NO. 2020-06-004). A total of 120 female ICR adult mice were randomly divided into six groups (n = 20): control group, model group (scopolamine), 5 mg/kg donepezil hydrochloride, 0.1 mg/kg **24r-HCl**, 0.3 mg/kg **24r-HCl** and 1 mg/kg **24r-HCl**. Then three separate trials were performed: training trial, learning trial and memory trial. The mice were given training trial on the first day: each mouse was put into the bright compartment with its back facing the door, and allowed to move freely in both the bright compartment and the dark compartment for 5 min. On the second day, the mice were given a learning trial after i.g. administration. Each mouse was put into the bright compartment with its back facing the door, and a timer was started at the same time. The mice were given an electric foot shock (0.19 mA) when they passed through the door to the dark compartment. The recorded time was defined as the latency time and the number of times the mice entered the dark compartment (the number of errors) within 5 minutes was recorded. At the same time, the latency time was recorded as 300 s when the mice did not enter the dark compartment for 5 minutes. The memory trial was conducted on the third day. The stimulator in the dark compartment was turned on. Each mouse was put into the bright compartment with its back facing the door, and the latency time and the number of errors within 5 minutes were still recorded. All data are expressed as the mean ± SEM and differences between groups were examined for statistical significance using one-way ANOVA with Student's t-test. A P-value less than 0.05 denoted the presence of a statistically significant difference.

Declaration of conflicting interest

The authors declare that they have no known conflicting financial interests or personal

relationships that could have appeared to influence the work reported in this paper.

Acknowledgments

The authors thank the funder of National Natural Science Foundation of China (No. 81874289) for financial support to conduct chemical synthesis and *in vivo* animal work, together with the funder of “Double First-Class" University project CPU2018GY04, China Pharmaceutical University and the funder of Fundamental Research Funds for the Central Universities (2632020ZD03).

The authors also acknowledge financial support from School of Pharmacy, the University of Nottingham and EPSRC Centre for Doctoral Training in Advanced Therapeutics and Nanomedicines (EP/L01646X) to conduct the cellular pharmacology studies.

Appendix A. Supplementary data

Supplementary data to this article can be found online at

References

[1] L. Wang, Bharti, R. Kumar, P.F. Pavlov, B. Winblad, Small molecule therapeutics for tauopathy in Alzheimer's disease: Walking on the path of most resistance, Eur. J. Med. Chem. 209 (2021) 112915.

[2] P. Zhang, S. Xu, Z. Zhu, J. Xu, Multi-target design strategies for the improved treatment of Alzheimer's disease, Eur. J. Med. Chem. 176 (2019) 228-247.

[3] C.J.A.s. Lynch, Dementia, World Alzheimer Report 2019: Attitudes to dementia, a global survey: Public health: Engaging people in ADRD research, 16 (2020) e038255.

[4] R. León, A.G. Garcia, J. Marco-Contelles, Recent advances in the multitarget-directed ligands approach for the treatment of Alzheimer's disease, Med. Res. Rev. 33 (2013) 139-189.

[5] H. Wang, H. Zhang, Reconsideration of anticholinesterase therapeutic strategies against Alzheimer's disease, ACS. Chem. Neurosci. 10 (2019) 852-862.

[6] S. Srivastava, R. Ahmad, S.K. Khare, Alzheimer's disease and its treatment by different approaches: A review, Eur. J. Med. Chem. 216 (2021) 113320.

[7] M. Singh, M. Kaur, H. Kukreja, R. Chugh, O. Silakari, D. Singh, Acetylcholinesterase inhibitors

as Alzheimer therapy: from nerve toxins to neuroprotection, Eur. J. Med. Chem. 70 (2013) 165-188.

[8] M. Scheiner, M. Hoffmann, F. He, E. Poeta, A. Chatonnet, B. Monti, T. Maurice, M. Decker, Selective pseudo-irreversible butyrylcholinesterase inhibitors transferring antioxidant moieties to the enzyme show pronounced neuroprotective efficacy in vitro and in vivo in an Alzheimer's disease Mouse Model, J. Med. Chem. 64 (2021) 9302-9320.

[9] Q. Li, Y. Chen, S. Xing, Q. Liao, B. Xiong, Y. Wang, W. Lu, S. He, F. Feng, W. Liu, Y. Chen, H. Sun, Highly potent and selective butyrylcholinesterase inhibitors for cognitive improvement and neuroprotection, J. Med. Chem. 64 (2021) 6856-6876.

[10] A. Kumar, A. Singh, Ekavali, A review on Alzheimer's disease pathophysiology and its management: an update, Pharmacol. Rep. 67 (2015) 195-203.

[11] Q. Li, S. He, Y. Chen, F. Feng, W. Qu, H. Sun, Donepezil-based multi-functional cholinesterase inhibitors for treatment of Alzheimer's disease, Eur. J. Med. Chem. 158 (2018) 463-477.

[12] L. Ismaili, B. Refouvelet, M. Benchekroun, S. Brogi, M. Brindisi, S. Gemma, G. Campiani, S. Filipic, D. Agbaba, G. Esteban, M. Unzeta, K. Nikolic, S. Butini, J. Marco-Contelles, Multitarget compounds bearing tacrine- and donepezil-like structural and functional motifs for the potential treatment of Alzheimer's disease, Prog. Neurobiol. 151 (2017) 4-34.

[13] E. Mezeiova, K. Chalupova, E. Nepovimova, L. Gorecki, L. Prchal, D. Malinak, K. Kuca, O. Soukup, J. Korabecny, Donepezil derivatives targeting amyloid-β cascade in Alzheimer's disease, Curr. Alzheimer. Res. 16 (2019) 772-800.

[14] E. Mezeiova, K. Spilovska, E. Nepovimova, L. Gorecki, O. Soukup, R. Dolezal, D. Malinak, J. Janockova, D. Jun, K. Kuca, J. Korabecny, Profiling donepezil template into multipotent hybrids with antioxidant properties, J. Enzyme. Inhib. Med. Chem. 33 (2018) 583-606

[15] J. Korabecny, K. Spilovska, E. Mezeiova, O. Benek, R. Juza, D. Kaping, O. Soukup, A systematic review on donepezil-based derivatives as potential cholinesterase inhibitors for Alzheimer's disease, Curr. Med. Chem. 26 (2019) 5625-5648.

[16] H. Nadri, M. Pirali-Hamedani, M. Shekarchi, M. Abdollahi, V. Sheibani, M. Amanlou, A. Shafiee, A. Foroumadi, Design, synthesis and anticholinesterase activity of a novel series of 1-benzyl-4-((6-alkoxy-3-oxobenzofuran-2(3*H*)-ylidene) methyl) pyridinium derivatives, Bioorg. Med. Chem. 18 (2010) 6360-6366.

[17] M. Alipour, M. Khoobi, A. Foroumadi, H. Nadri, A. Moradi, A. Sakhteman, M. Ghandi, A.

Shafiee, Novel coumarin derivatives bearing *N*-benzyl pyridinium moiety: potent and dual binding site acetylcholinesterase inhibitors, Bioorg. Med. Chem. 20 (2012) 7214-7222.

[18] H. Akrami, B.F. Mirjalili, M. Khoobi, H. Nadri, A. Moradi, A. Sakhteman, S. Emami, A. Foroumadi, A. Shafiee, Indolinone-based acetylcholinesterase inhibitors: synthesis, biological activity and molecular modeling, Eur. J. Med. Chem. 84 (2014) 375-381.

[19] F. Baharloo, M.H. Moslemin, H. Nadri, A. Asadipour, M. Mahdavi, S. Emami, L. Firoozpour, R. Mohebat, A. Shafiee, A. Foroumadi, Benzofuran-derived benzylpyridinium bromides as potent acetylcholinesterase inhibitors, Eur. J. Med. Chem. 93 (2015) 196-201.

[20] J.S. Lan, T. Zhang, Y. Liu, J. Yang, S.S. Xie, J. Liu, Z.Y. Miao, Y. Ding, Design, synthesis and biological activity of novel donepezil derivatives bearing *N*-benzyl pyridinium moiety as potent and dual binding site acetylcholinesterase inhibitors, Eur. J. Med. Chem. 133 (2017) 184-196.

[21] C. Wang, Z. Wu, H. Cai, S. Xu, J. Liu, J. Jiang, H. Yao, X. Wu, J. Xu, Design, synthesis, biological evaluation and docking study of 4-isochromanone hybrids bearing *N*-benzyl pyridinium moiety as dual binding site acetylcholinesterase inhibitors, Bioorg. Med. Chem. Lett. 25 (2015) 5212-5216.

[22] J. Wang, C. Wang, Z. Wu, X. Li, S. Xu, J. Liu, Q. Lan, Z. Zhu, J. Xu, Design, synthesis, biological evaluation, and docking study of 4-isochromanone hybrids bearing *N*-benzyl pyridinium moiety as dual binding site acetylcholinesterase inhibitors (part II), Chem. Biol. Drug. Des. 91 (2018) 756-762.

[23] G. Uras, A. Manca, P. Zhang, Z. Markus, N. Mack, S. Allen, M. Bo, S. Xu, J. Xu, M. Georgiou, Z. Zhu, *In vivo* evaluation of a newly synthesized acetylcholinesterase inhibitor in a transgenic Drosophila model of Alzheimer's disease, Front Neurosci. 15 (2021) 691222.

[24] M. Shidore, J. Machhi, K. Shingala, P. Murumkar, M.K. Sharma, N. Agrawal, A. Tripathi, Z. Parikh, P. Pillai, M.R. Yadav, Benzylpiperidine-linked diarylthiazoles as potential anti-Alzheimer's agents: synthesis and biological evaluation, J. Med. Chem. 59 (2016) 5823-5846.

[25] M.I. Rodríguez-Franco, M.I. Fernández-Bachiller, C. Pérez, A. Castro, A. Martínez, Design and synthesis of *N*-benzylpiperidine-purine derivatives as new dual inhibitors of acetyl- and butyrylcholinesterase, Bioorg. Med. Chem. 13 (2005) 6795-6802.

[26] A. Asadipour, M. Alipour, M. Jafari, M. Khoobi, S. Emami, H. Nadri, A. Sakhteman, A. Moradi, V. Sheibani, F. Homayouni Moghadam, A. Shafiee, A. Foroumadi, Novel coumarin-3-carboxamides

bearing *N*-benzylpiperidine moiety as potent acetylcholinesterase inhibitors, Eur. J. Med. Chem. 70 (2013) 623-630.

[27] Z. Luo, J. Sheng, Y. Sun, C. Lu, J. Yan, A. Liu, H.B. Luo, L. Huang, X. Li, Synthesis and evaluation of multi-target-directed ligands against Alzheimer's disease based on the fusion of donepezil and ebselen, J. Med. Chem. 56 (2013) 9089-9099.

[28] B.M. Johnson, Y.Z. Shu, X. Zhuo, N.A. Meanwell, Metabolic and pharmaceutical aspects of fluorinated compounds, J. Med. Chem. 63 (2020) 6315-6386.

[29] Y. Zhou, J. Wang, Z. Gu, S. Wang, W. Zhu, J.L. Aceña, V.A. Soloshonok, K. Izawa, H. Liu, Next generation of fluorine-containing pharmaceuticals, compounds currently in phase II-III clinical trials of major pharmaceutical companies: new structural trends and therapeutic areas, Chem. Rev. 116 (2016) 422-518.

[30] J. Wang, M. Sánchez-Roselló, J.L. Aceña, C. del Pozo, A.E. Sorochinsky, S. Fustero, V.A. Soloshonok, H. Liu, Fluorine in pharmaceutical industry: fluorine-containing drugs introduced to the market in the last decade (2001-2011), Chem. Rev. 114 (2014) 2432-2506.

[31] W.K. Hagmann, The many roles for fluorine in medicinal chemistry, J. Med. Chem. 51 (2008) 4359-4369.

[32] Y. Zhou, Y. Fu, W. Yin, J. Li, W. Wang, F. Bai, S. Xu, Q. Gong, T. Peng, Y. Hong, D. Zhang, D. Zhang, Q. Liu, Y. Xu, H.E. Xu, H. Zhang, H. Jiang, H. Liu, Kinetics-driven drug design strategy for next-generation acetylcholinesterase inhibitors to clinical candidate, J. Med. Chem. 64 (2021) 1844-1855.

[33] S.Y. Woo, J.H. Kim, M.K. Moon, S.H. Han, S.K. Yeon, J.W. Choi, B.K. Jang, H.J. Song, Y.G. Kang, J.W. Kim, J. Lee, D.J. Kim, O. Hwang, K.D. Park, Discovery of vinyl sulfones as a novel class of neuroprotective agents toward Parkinson's disease therapy, J. Med. Chem. 57 (2014) 1473-1487.

[34] J.W. Choi, S. Kim, J.H. Park, H.J. Kim, S.J. Shin, J.W. Kim, S.Y. Woo, C. Lee, S.M. Han, J. Lee, A.N. Pae, G. Han, K.D. Park, Optimization of vinyl sulfone derivatives as potent nuclear factor erythroid 2-related factor 2 (Nrf2) activators for Parkinson's disease Therapy, J. Med. Chem. 62 (2019) 811-830.

[35] X. Ning, Y. Guo, X. Wang, X. Ma, C. Tian, X. Shi, R. Zhu, C. Cheng, Y. Du, Z. Ma, Z. Zhang, J. Liu, Design, synthesis, and biological evaluation of (e)-3,4-dihydroxystyryl aralkyl sulfones and

sulfoxides as novel multifunctional neuroprotective agents, J. Med. Chem. 57 (2014) 4302-4312.

[36] Y. Chen, B. Wu, Y. Hao, Y. Liu, Z. Zhang, C. Tian, X. Ning, Y. Guo, J. Liu, X. Wang, Structure-activity relationship studies of (*E*)-3,4-dihydroxystyryl alkyl sulfones as novel neuroprotective agents based on improved antioxidant, anti-inflammatory activities and BBB permeability, Eur. J. Med. Chem. 171 (2019) 420-433.

[37] H. Liu, H. Zhang, Y. Fu, H. Jiang, X. Tang, K. Chen, Fluorine substituted cyclic amine compounds and preparation methods, pharmaceutical compositions, and uses thereof. 01 May, 2014. WO 2014/063587 A1.

[38] M.Y. Noh, S.H. Koh, Y. Kim, H.Y. Kim, G.W. Cho, S.H. Kim, Neuroprotective effects of donepezil through inhibition of GSK-3 activity in amyloid-beta-induced neuronal cell death, J. Neurochem. 108 (2009) 1116-1125.

[39] Y. Yoshiyama, A. Kojima, C. Ishikawa, K. Arai, Anti-inflammatory action of donepezil ameliorates tau pathology, synaptic loss, and neurodegeneration in a tauopathy mouse model, J. Alzheimers. Dis. 22 (2010) 295-306.

[40] H. Hampel, M.M. Mesulam, A.C. Cuello, M.R. Farlow, E. Giacobini, G.T. Grossberg, A.S. Khachaturian, A. Vergallo, E. Cavedo, P.J. Snyder, Z.S. Khachaturian, The cholinergic system in the pathophysiology and treatment of Alzheimer's disease, Brain. 141 (2018) 1917-1933.

[41] N.G. Norwitz, A.S. Mota, S.G. Norwitz, K. Clarke, Multi-loop model of Alzheimer disease: an integrated perspective on the Wnt/GSK3β, α-synuclein, and type 3 diabetes hypotheses, Front. Aging. Neurosci. 11 (2019).

[42] S. Jiang, Y. Li, C. Zhang, Y. Zhao, G. Bu, H. Xu, Y.W. Zhang, M1 muscarinic acetylcholine receptor in Alzheimer's disease, Neurosci. Bull. 30 (2014) 295-307.

[43] C. Ballatore, K.R. Brunden, D.M. Huryn, J.Q. Trojanowski, V.M. Lee, A.B. Smith, 3rd, Microtubule stabilizing agents as potential treatment for Alzheimer's disease and related neurodegenerative tauopathies, J. Med. Chem. 55 (2012) 8979-8996.

[44] B. Bulic, M. Pickhardt, E. Mandelkow, Progress and developments in tau aggregation inhibitors for Alzheimer disease, J. Med. Chem. 56 (2013) 4135-4155.

[45] P.K. Kamat, S. Tota, R. Shukla, S. Ali, A.K. Najmi, C. Nath, Mitochondrial dysfunction: a crucial event in okadaic acid (ICV) induced memory impairment and apoptotic cell death in rat brain, Pharmacol. Biochem. Behav. 100 (2011) 311-319.

[46] M. Rosini, E. Simoni, A. Milelli, A. Minarini, C. Melchiorre, Oxidative stress in Alzheimer's disease: are we connecting the dots?, J. Med. Chem. 57 (2014) 2821-2831.

[47] S. Zhao, X. Zhang, P. Wei, X. Su, L. Zhao, M. Wu, C. Hao, C. Liu, D. Zhao, M. Cheng, Design, synthesis and evaluation of aromatic heterocyclic derivatives as potent antifungal agents, Eur. J. Med. Chem. 137 (2017) 96-107.

[48] D. Wang, M. Hu, X. Li, D. Zhang, C. Chen, J. Fu, S. Shao, G. Shi, Y. Zhou, S. Wu, T. Zhang, Design, synthesis, and evaluation of isoflavone analogs as multifunctional agents for the treatment of Alzheimer's disease, Eur. J. Med. Chem. 168 (2019) 207-220.

[49] Z.P. Sang, X.M. Qiang, Y. Li, B. Wu, H. Zhang, M.G. Zhao, Y. Deng, Design, synthesis, and biological evaluation of scutellarein carbamate derivatives as potential multifunctional agents for the treatment of Alzheimer's disease, Chem. Biol. Drug. Des. 86 (2015) 1168-1177.

[50] M.M. Shipley, C.A. Mangold, M.L. Szpara, Differentiation of the SH-SY5Y human neuroblastoma cell line, J. Vis. Exp. (108), e53193.

[51] Y. Koriyama, A. Furukawa, M. Muramatsu, J. Takino, M. Takeuchi, Glyceraldehyde caused Alzheimer's disease-like alterations in diagnostic marker levels in SH-SY5Y human neuroblastoma cells, Sci. Rep. 5 (2015) 13313.